



# Furfural hydrogenation over Cu, Ni, Pd, Pt, Re, Rh and Ru catalysts: *Ab initio* modelling of adsorption, desorption and reaction micro-kinetics

Rok Šivec<sup>a,b</sup>, Matej Huš<sup>a,b,c</sup>, Blaž Likozar<sup>a,d,e</sup>, Miha Grilc<sup>a,b,\*</sup>

<sup>a</sup> Department of Catalysis and Chemical Reaction Engineering, National Institute of Chemistry, Hajdrihova 19, 1000 Ljubljana, Slovenia

<sup>b</sup> University of Nova Gorica, Vipavska 13, SI-5000 Nova Gorica, Slovenia

<sup>c</sup> Association for Technical Culture (ZOTKS), Zaloška 65, SI-1000 Ljubljana, Slovenia

<sup>d</sup> Pulp and Paper Institute, Bogišičeva 8, 1000 Ljubljana, Slovenia

<sup>e</sup> Faculty of Polymer Technology, Ozare 19, SI-2380 Slovenj Gradec, Slovenia

## ARTICLE INFO

### Keywords:

Furfural hydrogenation  
Tetrahydrofurfuryl alcohol  
Micro-kinetic mass transfer model  
Carbon based catalysts  
First-principle methods  
Lignocellulosic biomass

## ABSTRACT

Hydrogenation, hydrodeoxygenation and ring opening of biomass-derived furfural were studied by using Pd/C, Pt/C, Re/C, Ru/C, Rh/C, Ni/C and Cu/C catalysts. Based on experiments, a generalized micro-kinetic model was developed, describing kinetics of tested catalysts well. Pd/C could unselectively hydrogenate furfural's ring, aldehyde group or both and was the most active tested catalyst. Selective aldehyde group hydrogenation, followed by deoxygenation was observed with other catalysts. This route was also favorable thermodynamically according to density functional theory (DFT) calculations. Only Ru/C could form methyltetrahydrofuran (45.3 % yield) and ring opening products at 200 °C. Reaction conditions were optimized *in silico* for most promising catalysts (Pd, Pt, Re, Ni on carbon), by fixing the kinetic parameters obtained by regression analysis and subsequently maximizing the objective function, i.e. the yield of the product of interest. Validation experiments confirmed a high Pd/C hydrogenation activity already at 40 °C, forming predominantly tetrahydrofurfural (85 % yield), while 95 % yield of 2-methyltetrahydrofuran was obtained by using a cheap Ni/C at 212 °C.

## 1. Introduction

In recent years, a growing trend towards the use of renewable sources has materialized as replacements of petroleum-based fuels and chemicals are being incentivized. Lignocellulosic biomass remains one of the most abundant renewable and sustainable sources. Its main constituents are cellulose, hemicellulose and lignin, which can be valorized in different ways: e.g. gasification, pyrolysis and hydrolysis [1].

Some platform chemicals, such as furfural (FUR), are already produced in large quantities through acid-catalyzed hydrolysis and subsequent dehydration of sugars [2–4]. FUR was also listed by the US Department of Energy as one of the most important platform chemicals [5,6]. Various heterogeneous catalysts have been tested for the transformation of FUR towards a wide range of products, some of which could replace oil-based chemical in various industries as a greener alternative [7–13].

Metallic catalysts – such as Ni, Pd, Pt, Cu, Ru, Re, and Rh – exhibit hydrogenation hydrodeoxygenation, and/or decarbonylation activity when hydrogen gas and/or hydrogen donor solvent is used. Commonly

used solvents include various alcohols (2-propanol, ethanol, methanol), which can act as proton donors and can in some cases serve also as hydrogen donors as a replacement for gaseous hydrogen. A possible downside is the intrinsic reactivity of these solvents, possibly forming ethers or other side products with FUR and its derivatives. This is caused by slower hydrogenation reactions in comparison to using gaseous hydrogen as a hydrogen source [14–16].

Ni-based catalysts showed good activity for the hydrogenation of the aromatic ring or/and aldehyde group, making them useful for the selective conversion of FUR to tetrahydrofurfuryl alcohol (THFA) [17–28]. However, leaching of Ni in liquid phase needs to be resolved [26]. Pd and Pt catalysts strongly adsorb C<sub>sp</sub><sup>2</sup> containing hydrocarbons and are active for the aromatic ring hydrogenation [29–31]. Pd catalysts exhibit high hydro(deoxy)genation activity and good catalyst stability. It can be used for transforming FUR to THFA, furfuryl alcohol (FA) and also 2-methylfuran (MF), depending on the operating conditions [19,20,32–40]. Pt catalysts on the other hand showed similar adsorption properties but are more active for the hydrogenation of side groups not the aromatic ring. As a result, FA, MF and furan are observed as the main

\* Corresponding author.

E-mail address: [miha.grilc@ki.si](mailto:miha.grilc@ki.si) (M. Grilc).

<https://doi.org/10.1016/j.cej.2022.135070>

Received 9 November 2021; Received in revised form 19 January 2022; Accepted 31 January 2022

Available online 4 February 2022

1385-8947/© 2022 The Author(s). Published by Elsevier B.V. This is an open access article under the CC BY license (<http://creativecommons.org/licenses/by/4.0/>).

products [35,41–49]. While FUR generally adsorbs in a flat orientation, it was suggested that it shifts to a tilted orientation at higher surface coverages [41]. Cu-based catalysts have shown high selectivity for the hydrogenation of the carbonyl group and subsequent hydrodeoxygenation only at elevated temperatures ( $>230\text{ }^{\circ}\text{C}$ ) [17,27,50–53]. DFT calculations have shown that FUR adsorbs primarily through the interaction of its  $\pi$  electrons on extended Cu surfaces [54]. Ru-based catalysts have shown promising results for the production of FA under milder reaction conditions [55–57]. The reactions are structure-sensitive, as the selectivity shifts when differently sized Ru nanoparticles were used [57]. It was also found that the increased hydrogen/FUR ratio shifts the mechanism towards hydrogenation, producing tetrahydrofurfural [58]. Production of 2-methylfuran over Ru/C can also be achieved at higher temperatures in liquid phase through the catalytic transfer hydrogenation in isopropanol [59]. Rh catalysts [60–63] also exhibit high hydrogenation activity to THFA through FA. Rh/C catalysts showed the highest selectivity towards THFA in water, compared to Ni/C, Ru/C and Pd/C [63]. 1 % Re on  $\text{TiO}_2\text{-ZrO}_2$  support hydrogenated the C = O group in ethanol with a 57.6 % selectivity towards FA, 29.1 % to acetal and 13.3 % to other products [19]. Bimetallic catalysts also showed synergistic effects in combination with other metals. A bimetallic Pt-Re catalyst was used to produce FA in ethanol with a 95.7 % yield [19], while Rh- $\text{ReO}_x/\text{SiO}_2$  [54] and Rh-Ir- $\text{ReO}_x/\text{SiO}_2$  [64] catalyst favored ring-opening reactions.

Microkinetic modelling gives better insight into the reaction mechanics and helps quantify the influence of reaction conditions. Several first-principles methods exist for calculating the parameters of chemical reactions on the catalytic surfaces [65]. They have been used in studying acidic hydrolysis of biomass or its valorization by using solid catalysts [52,66–75]. A limited number of first-principles studies were conducted on FUR valorization. For instance, the effects of hydrogen coverage on Pd(111) [71], shape and size of Pt particles (Pt(111), Pt(211) and Pt<sub>55</sub> cuboctahedron) [72], the reaction mechanism on Ru(0001) and RuO<sub>2</sub>(110) [73,74], the effect of varying surface coverage on Mo<sub>2</sub>C [52], the reaction mechanism on MoO<sub>2</sub>(111), MoO<sub>3</sub>(101) and MoO<sub>3</sub>(111) [76], the mechanism of hydrogenation (FUR to FA) over Cu(111), CuO(100) and Cu<sub>2</sub>O(100) [77] were studied and compared to the experimental results.

In our previous study, a microkinetic model for the conversion of FUR over a Pd/C catalyst was developed [32]. It was shown that mass transfer limitations can greatly influence the conversion and selectivity towards FA or THFA on a Pd/C catalyst when using isopropanol or THF as a solvent. Although isopropanol was somewhat active as a proton donor, the reactions with dissolved hydrogen were found to be much faster, leading to comparable reaction rates in both solvents.

In this work, a thorough experimental and computational study of furfural hydrogenation, deoxygenation, and ring opening reactions over various catalysts (Ni/C, Pd/C, Pt/C, Cu/C, Ru/C, Rh/C, Re/C) was conducted, by using tetrahydrofuran as a solvent and gaseous hydrogen as hydrogenation agent. A model was developed to obtain adsorption and desorption kinetics parameters, based on the temperature programmed desorption of carbon monoxide (CO-TPD). Our previously developed mechanistic micro-kinetic model was expanded for all tested catalysts. Quantum calculations, based on plane-wave density functional theory (DFT) were used to explain reaction mechanics and thermodynamics. The micro-kinetic model was used to optimize reaction conditions for four most promising catalysts. Predictions were also experimentally validated.

## 2. Methods

### 2.1. Materials

Gaseous hydrogen (5.0, Messer, Gumpoldskirchen, Austria) was used for catalyst reduction and as the main reactant. Liquid furfural (99 %, Sigma-Aldrich, St Louis, MO, USA, reference number 185914) was used

as the main reactant, and tetrahydrofuran (THF) for analysis ( $\geq 99.8\%$ , Merck KGaA, Darmstadt, Germany, reference number 1097312500) was used as a solvent. Nitrogen gas (5.0, Messer, Gumpoldskirchen, Austria) was used to flush the reactor before and after experiments. 5 % hydrogen in argon (Messer, Ruše, Slovenia) was used for catalyst reduction during the H<sub>2</sub>-TPD and CO-TPD measurements. Mesoporous carbon (Sigma-Aldrich, St Louis, MO, USA, reference number 702102) was used in the blank run, while other commercially available catalysts, such as 5 % palladium on activated carbon catalyst (Degussa, type E190 NW/W with 50 % water content), 5 % platinum on carbon (Sigma-Aldrich, St Louis, MO, USA, reference number 205931), 5 % ruthenium on carbon (Sigma-Aldrich, St Louis, MO, USA, reference number), 5 % rhenium on carbon (Riogen, NJ, USA), 5 % rhodium on carbon (Riogen, NJ, USA), 2–5 mm pellets of 5 % nickel on carbon (Riogen, NJ, USA), 2–5 mm pellets of 5 % copper on carbon (Riogen, NJ, USA) were used. Nickel and copper on carbon catalysts were ground and sieved before the use to obtain 40–100  $\mu\text{m}$  fraction, while other catalysts were used in the powder form as purchased.

### 2.2. Catalyst characterization

X-ray diffraction (XRD) analysis of all fresh, unreduced catalysts was conducted in the  $2\theta$  range of  $5^{\circ}$  to  $90^{\circ}$  with a  $0.001^{\circ}$  minimum step size on PANalytical X'Pert PRO instrument, by using  $\text{CuK}\alpha$  (5 kW, 45 mA) as radiation source ( $\lambda = 0.154056\text{ nm}$ ), with a Ni filter for  $\text{K}\beta$  radiation.

ASAP 2020 gas adsorption instrument (Micrometrics, Norcross, GA, USA) was used to obtain nitrogen adsorption–desorption isotherms. Nitrogen physisorption measurements were performed, to calculate BET specific surface area ( $S_{\text{BET}}$ ), single point adsorption total volume of pores ( $V_p$ ) and adsorption average pore diameter ( $d_p$ ). The volume ( $V_{\text{micro}}$ ) and area ( $A_{\text{micro}}$ ) in pores, smaller than 15 nm, was determined by using NLDFT method.

Micrometrics AutoChem II Chemisorption Analyser (Micrometrics, Norcross, GA, USA) was used for temperature programmed reduction with hydrogen (H<sub>2</sub>-TPR) to observe the reduction properties of the catalyst, while temperature programmed desorption of carbon monoxide (CO-TPD) was used to determine the concentration of active metal sites. Approximately 100 mg of catalyst was weighted into a quartz U-tube. The sample for H<sub>2</sub>-TPR was heated up to  $300\text{ }^{\circ}\text{C}$  with a heating rate of  $30\text{ K min}^{-1}$  under  $50\text{ mL min}^{-1}$  flow of argon. The temperature plateau was held for 30 min prior reduction. After the cooldown, a constant  $40\text{ mL min}^{-1}$  flow of 5 vol% of H<sub>2</sub> in Ar was introduced. The sample was heated up to  $800\text{ }^{\circ}\text{C}$  with a heating rate  $10\text{ K min}^{-1}$ . A TCD detector was used to determine hydrogen consumption.

Catalyst samples for CO-TPD measurements were first reduced by using  $40\text{ mL min}^{-1}$  flow of 5 vol% of H<sub>2</sub> in Ar. The sample was heated up to  $400\text{ }^{\circ}\text{C}$  with a heat up rate of  $10\text{ K min}^{-1}$  and held for 3 h. After cooling down to room temperature, the sample was flushed with He, saturated with carbon monoxide (5 vol% CO in He) and flushed again with He prior heating up to  $800\text{ }^{\circ}\text{C}$ , with a heat up rate of  $10\text{ K min}^{-1}$ . MS detector was used to determine the amount of desorbed CO. 28  $m/z$  and 44  $m/z$  signal were calibrated by using five CO and five CO<sub>2</sub> pulses after each measurement.

### 2.3. Quantum calculations

Theoretical calculations were performed using the plane-wave density functional theory (DFT) framework in VASP. Electron-ion interactions were described with the projector-augmented wave (PAW) approach and the RPBE exchange–correlation functional. For well converged results, an energy cutoff of 450 eV was sufficient. Since van der Waals interactions play a crucial role in the adsorption of (saturated) hydrocarbons on metallic surfaces, the Grimme D3 approach was used to supplement the flawed DFT treatment of the dispersion interaction. For nickel, spin-polarized calculations were required. The geometry optimizations were performed until the forces dropped below  $0.03\text{ eV}/\text{\AA}$ .

The following metals were probed as catalysts: Cu, Ni, Pd, Pt, Re, Rh, Ru. Among those, Re and Ru assume the hcp structure, while the remaining ones crystallize in fcc. For each catalyst, the lattice parameters were determined by optimizing the volume of their unit cell with respect to energy, using a  $16 \times 16 \times 16$  Monkhorst-Pack mesh. From the optimized bulk structure, four-layer slabs of extended surfaces (fcc(111) or hcp(0001)) were cut off. A  $4 \times 4$  supercell was required to accommodate the intermediates with enough lateral spacing as to minimize the cross-cell interactions. A  $2 \times 2 \times 1$  Monkhorst-Pack mesh was sufficient for such large supercells.

On the slabs, the bottom two layers were kept fixed to approximate the bulk. Stable furfural-derived intermediates were adsorbed on the surfaces. For each compound, nine possible surface orientations were investigated to locate the most stable one. While small fragments (such as  $\text{CH}^*$ ) assume well-defined surface sites (fcc, hcp, top, bridge), larger molecules cannot. Thus, the nine orientations were constructed by translating and rotating the molecules at the surface.

For the lowest-lying structure, the adsorption energy was calculated as  $E_{\text{ads}} = E_{\text{slab/ads}} - E_{\text{slab}} - E_{\text{gas}}$ , where  $E_{\text{slab/ads}}$  stands for the energy of the slab with the adsorbate,  $E_{\text{slab}}$  is the energy of the empty slab and  $E_{\text{gas}}$  is the energy of the relaxed gaseous adsorbate.

## 2.4. Catalytic tests

All experiments were conducted in a batch three-phase system, which consists of 250 mL stainless steel reactor vessels with a magnetically driven Rushton turbine impeller (with 30 mm diameter and positioned 25 mm above the reactor bottom), a heating jacket and a water cooling system. The reactor vessel is equipped with on-line temperature and pressure probes and regulated through SCADA software. All experimental runs are presented in Table 1. Seven different metal catalysts and carbon support were tested. Each metal catalyst was reduced for 4 h at 400 °C prior to the reaction in a tube furnace by using a 200 mL  $\text{min}^{-1}$  flow of pure hydrogen. After cooling down, the catalyst was carefully transferred in inert atmosphere to the reactor mixture,

**Table 1**

Operating conditions used in each experiment. 0.2 wt% of catalyst, 5 wt% of furfural, 94.8 wt% of tetrahydrofuran and 60 bar of pure hydrogen at room temperature were used in a typical experiment. All experiments started at room temperature.

Run	Catalyst/support	$T$ (°C)	$N$ ( $\text{min}^{-1}$ )
1	5 % Pd/C	100	1000
2	5 % Pd/C	100	1200
3	C	100	1000
4	5 % Ni/C	100	1000
5	5 % Cu/C	100	1000
6	5 % Ru/C	100	1000
7	5 % Rh/C	100	1000
8	5 % Pt/C	100	1000
9	5 % Re/C	100	1000
10	5 % Ni/C	150	1000
11	5 % Cu/C	150	1000
12	5 % Pd/C	150	1000
13	5 % Ru/C	150	1000
14	5 % Rh/C	150	1000
15	5 % Pt/C	150	1000
16	5 % Re/C	150	1000
17	5 % Ni/C	200	1000
18	5 % Cu/C	200	1000
19	5 % Pd/C	200	1000
20	5 % Ru/C	200	1000
21	5 % Rh/C	200	1000
22	5 % Pt/C	200	1000
23	5 % Re/C	200	1000
24	5 % Pd/C	40	1000
25	5 % Pt/C	220	1000
26	5 % Re/C	155	1000
27	5 % Ni/C	212	1000

which has been previously purged with argon to avoid oxidation. Pd/C catalyst was also dried at 110 °C prior to reduction due to high water content. The reaction mixture was heated from room temperature up to 100 °C, 150 °C or 200 °C. Typically, 0.2 g of catalyst, 5 g of furfural, 94.8 g of tetrahydrofuran and 60 bar of pure hydrogen were used to assure hydrogen in excess, while setting the stirring speed ( $N$ ) to 1000  $\text{min}^{-1}$ . A higher stirring speed of 1200  $\text{min}^{-1}$  was tested in Run 2 to test if external mass transfer limitations can be neglected. The liquid samples were taken directly from the reactor system by using equipped sampling tubes. The first sample was taken prior starting the reaction, the second one after the temperature ramp was reached, while the following samples were taken at 30 min intervals. The final sample was taken after the reaction mixture was flushed with nitrogen and cooled down.

## 2.5. Sample analysis

All liquid samples were collected at pre-determined reaction times during the reaction and were then filtered and diluted 25 times with tetrahydrofuran. Diluted samples were analyzed off-line by using gas chromatograph with flame ionization detector (GC-FID) (Thermo Fisher Scientific, Waltham, MA, USA) for quantification, coupled with mass spectrometer detector (GC-MS) (2010 Ultra, Shimadzu, Kyoto, Japan) for identification. GC-MS was also used for quantification of THFUR (71  $m/z$  signal) and FUR (67  $m/z$  signal) in cases where THFUR was detected, as their peaks were overlapping in a chromatogram. The stabilizer 2,6-di-tert-butyl-4-methylphenol (BHT) was used as an internal standard.

## 2.6. Mechanistic description of temperature programmed desorption

A fixed-bed reactor model was developed, which describes the adsorption and desorption of carbon monoxide to/from the catalyst surface, in order to fit CO-TPD data. The catalyst bed dimensions were 0.44 cm of height and 1.1 cm diameter. Bed porosity of 0.35 was estimated in order to calculate the volume of the gas phase ( $V_{\text{gas}}$ ) inside the catalyst bed. The average value of  $0.35 \pm 0.03$  was determined by 10 independent virtual packings (in the open-source software Blender) of randomly-shaped catalyst particles, with Gaussian particle size distribution (Figure S1), by following the methodology reported in our previous work [78]. The exactly same bed porosity of packed bed ( $0.35 \pm 0.03$ ) were reported for cylindrical particles by Flaischlen *et al.* [79] and Eppinger *et al.* [80]. The concentration of carbon monoxide in the inlet was set to zero and surface coverage of CO was initially set to 1 (total coverage of the catalyst surface) as starting conditions. The linear velocity in the axial direction of the gas ( $v$ ) was obtained by multiplying the measured flow rate of He (25  $\text{cm}^3 \text{min}^{-1}$  at ambient conditions) with a temperature correction factor (based on the ideal-gas approximation) and dividing it with a cross section of the reactor and bed porosity. The molar balance equations, used in the model are shown in equations (1) and (2), where time ( $t$ ) and axial coordinate ( $x$ ) were used as independent variables, while other variables were defined as follows: concentration of carbon monoxide in the gas phase ( $C_{\text{CO}}$ ), surface coverage with carbon monoxide ( $\theta_{\text{CO}}$ ), adsorption rate ( $k_{\text{ads}}$ ), desorption rate ( $k_{\text{des}}$ ) and number of total active sites ( $n_{\text{TS}}$ ). Desorption rate was temperature ( $T$ ) dependent according to Arrhenius law.

The 28  $m/z$  signals, obtained by CO-TPD were subtracted by the baseline. All the signals were then recalculated as the concentration of CO ( $C_{\text{CO}}$ ) in the outflow for each measurement, by using the calibration curve.

$$\frac{\partial C_{\text{CO}}}{\partial t} = -v \cdot \frac{\partial C_{\text{CO}}}{\partial x} - k_{\text{ads}} \cdot C_{\text{CO}}(x) \cdot (1 - \theta_{\text{CO}}(x)) + k_{\text{des}}(T) \cdot \theta_{\text{CO}}(x) \cdot \frac{n_{\text{TS}}}{V_{\text{gas}}} \quad (1)$$

$$\frac{\partial \theta_{\text{CO}}(x)}{\partial t} = k_{\text{ads}} \cdot C_{\text{CO}}(x) \cdot (1 - \theta_{\text{CO}}(x)) \cdot \frac{V_{\text{gas}}}{n_{\text{TS}}} - k_{\text{des}}(T) \cdot \theta_{\text{CO}}(x) \quad (2)$$

The total number of active sites, initial surface coverage, desorption

energy, adsorption and desorption rate constants were obtained by fitting the CO-TPD profiles for each catalyst, (excluding Cu due to a very low CO desorption temperature). We used literature data [81] as a proxy to fit these parameters in the case of Cu/C catalyst. The concentration of active sites is calculated by dividing the number of active sites with the mass of the catalyst. These parameters were used in the micro-kinetic model as an approximation for all furanic species in combination with each tested catalyst. Matlab software was used for coding and solving partial differential equations as a set (for every  $\times$  dimension-step) of ordinary differential equation by using an integrated Matlab solver (ode15s). Nelder–Mead method with objective function (sum of squared residuals) was used for regression analysis to estimate the relevant parameters.

## 2.7. Microkinetic modelling of the reaction pathway

The previously developed microkinetic model was generalized, expanded and improved, according to the reaction pathway network shown in Fig. 1. For details on the methodology, the reader is referred to Ref. [32]. Unless stated otherwise, the same assumptions apply. All reactions were assumed to follow the Langmuir–Hinshelwood mechanism.

In the first step the aldehyde group (with the rate constant  $k_1$ ) or the aromatic ring ( $k_2$ ) can undergo hydrogenation, leading to FA or THFUR, respectively. THFUR can be further hydrogenated to THFA ( $k_3$ ) and lastly to MTHF ( $k_6$ ). Should FA form, it can either undergo ring hydrogenation to THFA ( $k_4$ ) or deoxygenation to MF ( $k_5$ ). Ultimately, MTHF is the fully hydrogenated species ( $k_7$ ).

Various open ring products (OR), which were detected, were assumed to mostly form from FA. No reactions with the solvent were observed. Oligomerization products were only observed in low quantities in all tests (<2 wt%) and were therefore neglected in the model.

External mass transfer, hydrogen dissolution in the liquid phase, adsorption and desorption of each specie to the catalyst surface were accounted for in the model. The reactions were assumed not to be limited by hydrogen mass transport due to excess hydrogen and rapid stirring, as was also confirmed by varying stirring speed tests with the Pd/C catalyst (Run 1 and 2, shown in Table 1). As a result, hydrogen gas–liquid transfer parameters ( $k_{la}$ ) were high enough not to limit the

reaction rates, as reported in our previous work [82]. Adsorption and desorption parameters, were obtained by fitting CO-TPD data as previously described.

A set of ordinary differential equations was solved with an integrated Matlab solver (ode15s). The parameter optimization was performed using the Nelder–Mead method with the sum of squared residuals an objective function. Afterwards, Levenberg–Marquardt algorithm was used for a fine optimization and the computation of 95 % nonlinear regression confidence intervals for each parameter. The determined values were further used to calculate the TOF values (Eq. S1, Supplementary material) with the corresponding confidence intervals.

Kinetic parameters were obtained for each reaction (i) by first fitting reaction rate constants at 100 °C, while activation energies were fitted simultaneously for three catalytic tests at 100 °C, 150 °C and 200 °C for each individual catalyst. Reaction rate constants and activation energies were fitted again simultaneously at all tested temperature for each catalyst. Maximum turnover frequency (TOF) was calculated for each reaction step and was compared between the tested catalysts. Note, that TOF values were determined by the model after the regression analysis and optimal fitting of the experimental data.

## 3. Results and discussion

### 3.1. Catalyst characterisation

As shown in Table 2, Pd/C and Pt/C catalysts both showed superior specific surface area and pore volume. All catalysts exhibited micro- and mesoporous structure (Figure S2. and S3.). The average pore diameter was in all catalysts relatively similar (2.2 to 4.0 nm). Pores, smaller than 15 nm, were found to represent the majority of pore volume and surface area in all tested catalysts, as expected for carbon support.

An XRD spectra was also obtained to get insight into the bulk structure of fresh catalysts (Figure S4.). H<sub>2</sub>-TPD was conducted, to examine the reducibility of each catalyst. It is seen in Figure S5., that indeed all used catalysts can be reduced at 400 °C. The carbon support can decompose or react at temperatures above 550 °C. CO was assumed to desorb from metal surfaces below 450 °C, while CO can be formed and desorbed from carbon support also above this temperature, as was evident from the CO desorption peak for pure carbon support.

### 3.2. Liquid sample analysis

All species, shown in Fig. 1 were identified by GC–MS and quantified by GC–FID. FA, THFUR, THFA, MF and MF were the main observed products. Pentane-2-one, butan-1-ol, butane-1,4-diol and pentan-2-ol were also observed with Ru/C catalyst. Although some oligomerization products were detected, they were generally detected in low concentrations in all tests (<2 wt%). It is possible that some volatile products, such as furan or THF formed during the reaction, but was overlapped by the solvent peak and therefore excluded from reaction scheme. However, noticeable decarbonylation is reported to occur only at 200 °C or above [35], and was proved negligible by the gas phase analysis.

**Table 2**  
Textural properties of all tested catalysts.

Catalyst	$S_{\text{BET}}$ ( $\text{m}^2 \text{g}^{-1}$ )	$V_p$ ( $\text{cm}^3 \text{g}^{-1}$ )	$d_p$ (nm)	$V_{\text{micro}}$ (%)	$A_{\text{micro}}$ (%)
Carbon	572.0	0.4	2.5	92.8	99.0
Pd/C	1578.2	1.0	2.6	96.1	99.5
Pt/C	1529.5	1.3	3.5	92.4	99.2
Re/C	706.1	0.6	3.5	81.6	97.9
Ru/C	780.4	0.8	4.0	77.5	97.2
Rh/C	1057.4	0.6	2.2	97.8	99.9
Ni/C	996.4	0.6	2.3	96.6	99.8
Cu/C	1076.7	0.6	2.3	96.5	99.8

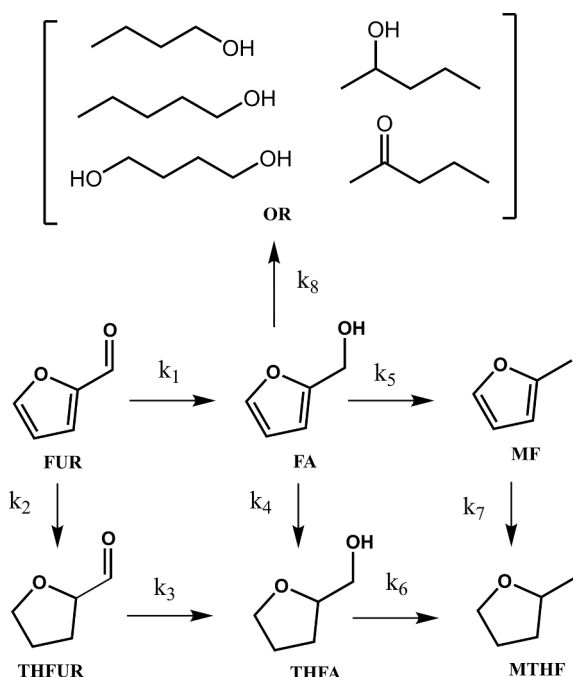


**Fig. 1.** General reaction pathway network for furfural hydrogenation over metal catalysts. Only stable intermediates and products are presented.

### 3.3. Theoretical calculations

At the atomistic level, the heterogeneously-catalyzed reactions are influenced by the electronic effects on the catalyst surface. Although being a first step in a reaction cascade, adsorption of the reactants (and intermediates and products) is paramount. In Table 3, we list the calculated binding strength (adsorption energies) of all stable intermediates and atomic hydrogen on the investigated model catalysts.

First, we see that the metals can be grouped into three types based on their affinity to bind hydrocarbons. Cu binds them poorly, while Pt, Re and Ru bind them strongly. Ni and Pd lie in-between. Upon closer inspection, we conclude that furfural adsorbs planarly with the ring parallel to the catalyst surface, which is a consequence of the interaction between its delocalized  $\pi$  electrons with the transition metal of the catalyst. However, the distance to the surface and the orientation of the carbonyl or aldehyde group vary (Fig. 2). It is in contact with Re, Ru, Rh, Ni, and Cu with the aromatic ring, the carbonyl and aldehyde groups. On Pd and Pt, its oxygen atoms are tilted away from the surface. Energetically, it adsorbs most strongly on Ru (-2.06 eV), followed by Pt > Re > Rh > Pd > Ni > Cu. The most abundant product, furfuryl alcohol, is most strongly bound to Pt (-2.20 eV), followed by Rh > Re > Ru > Pd > Cu > Ni.

An important characteristic is also the strength of hydrogen adsorption, which is strongest on Re and modestly strong on Pd, Ru, Rh and Ni, all the latter being known as good catalysts for hydrogenation.

This is consistent with the experimental results. At low temperatures, Pd is the most active (although poorly selective catalyst), followed by Ru. It would appear that Re binds hydrogen too strongly. At increased temperatures, Re, Rh and Ni all showed high catalytic activity.

For a broader picture, the thermodynamically most favorable pathways were evaluated by constructing the potential energy surface (PES) diagrams. Shown in Fig. 3 (see Table S1. for the numerical values), it displays the energetics of the adsorbed reactants, intermediates and products. Two competing pathways with possible interconversion are presented. Namely, the hydrogenation of FUR can first proceed by the degradation of the aldehyde group, yielding FA and MF, or by ring hydrogenation, yielding THFUR and THFA. FA can convert to THFA, as well. The fully hydrogenated product is MTHF. Aldehyde group hydro (deoxy)genation is more favorable than initial ring hydrogenation on Pd, Pt, Re, Ru, Rh and Ni, while Cu shows the opposite trend. According to experimental results, this pathway was followed on most of the tested catalysts, where FA and MF were the principal products. Some ring hydrogenation was only observed at the highest tested temperatures, while total hydrogenation (yielding MTHF) together with deoxygenation only occurred on Ru/C at 200 °C. At lower temperatures, only Pd forms noticeable amounts of the hydrogenated-ring products. Looking at the calculated thermodynamics, Pd is the only catalyst where the intermediates have roughly the same energies, meaning that there is no thermodynamic force favoring exclusive production of any of them. Although the potential diagram on Pt looks similar, the reaction from

**Table 3**

Adsorption energies of furfural, its derivatives, H<sub>2</sub>O and atomic hydrogen (H) on extended Pd(111), Pt(111), Re(0001), Ru(0001), Rh(111), Ni(111) and Cu(111) surfaces. For H, the values for two sites (hcp, fcc) are listed, both relative to ½ H<sub>2</sub> (g).

$E_{\text{ads}}$ (eV)	Pd	Pt	Re	Ru	Rh	Ni	Cu
FUR	-1.36	-1.94	-1.89	-2.06	-1.71	-1.29	-0.95
FA	-1.53	-2.20	-1.84	-1.78	-1.94	-1.04	-1.11
THFUR	-1.01	-1.01	-1.74	-1.41	-1.14	-0.92	-1.05
THFA	-1.02	-1.09	-1.24	-1.06	-1.02	-1.00	-1.05
MF	-1.18	-1.45	-1.20	-1.15	-1.27	-1.05	-1.03
MTHF	-0.95	-1.06	-1.07	-0.89	-0.96	-0.98	-1.03
H-fcc	-0.55	-0.45	-0.72	-0.58	-0.54	-0.52	-0.26
H-hcp	-0.50	-0.39	-0.73	-0.52	-0.52	-0.51	-0.26
H <sub>2</sub> O-top	-0.38	-0.41	-0.57	-0.52	-0.46	-0.45	-0.41

adsorbed FUR towards adsorbed FA is slightly exothermic in contrast to the strongly endothermic reaction towards adsorbed THFA, which could explain the lack of any hydrogenated-ring products on Pt.

Moreover, the tested catalysts vary in their interaction with different intermediates, thereby influencing the most favourable reaction pathway. The differences can be drastic. For instance, on Cu all hydrogenation reactions are exothermic because the reactants are adsorbed less strongly than the products, while on Ru the opposite is true. While the surface reaction is strongly exothermic on Cu, it proceeds slowly due to weak interactions of FUR and hydrogen with the catalyst. On the contrary, the reaction is strongly endothermic on Re, Ru and to a lesser extent on Rh. Only on Pd and Pt is the reaction roughly athermic. This explains why Pd and Pt perform well at lower temperatures, as well.

### 3.4. CO adsorption and desorption kinetics.

Regression analyses of CO-TPD profiles for each tested catalyst (Fig. 4) allowed calculating the concentration of surface sites and desorption kinetics parameters.

The total number of active (metallic) sites ( $n_{\text{TS}}$ ), activation energy of desorption ( $E_{\text{des}}$ ) and desorption rate constants ( $k_{\text{des}}$ ) were obtained by fitting the carbon monoxide concentration in the chemisorber outlet, which is based on the 28  $m/z$  signal. The concentration of active sites ( $C_{\text{AS}}$ ) was calculated by dividing  $n_{\text{TS}}$  (equivalent of moles of one desorbed CO molecule from each surface site) with the mass of the catalyst (see Table S2). Desorption rate constant increases with temperature (based on  $E_{\text{des}}$  according to the Arrhenius law), resulting in gradual desorption of CO from sites previously saturated at low temperature. Pre-exponential constant ( $A_{\text{des}}$ ) were calculated from obtained desorption rate constants according to Arrhenius law. The results are summarized in Table 4. It was found that kinetic parameters for CO desorption (particularly energy barrier required for CO desorption) generally followed the trend of adsorption energies of furanics determined by DFT (Table 3). Specifically; CO (and FUR) is/are strongly bond to Ru surface, while the interaction with Cu is by far the lowest.  $E_{\text{des}}$  of CO for other metals lie within  $36 \pm 8 \text{ kJ mol}^{-1}$ . Adsorption rate ( $k_{\text{ads}}$ ) was determined to be much higher, specifically in the range of  $1.7 \cdot 10^8 \text{ s}^{-1}$  for all cases and with negligible temperature dependence. Figure S6 demonstrates that the kinetic parameters for desorption (in particular  $E_{\text{des}}$ ) reported in Table 4 are independent from the initial surface coverage, as various initial values manage to fit the experimental CO-TPD profile equally well, as long as the initial surface coverage is sufficient (estimated as  $\theta_{\text{CO}}^i$  in Table 4) to account for the chemisorbed storage capacity of CO. After exceeding this value, the model predicts a slow but gradual desorption of physisorbed or weakly chemisorbed CO, observed before the heat-up ramp, while the crucial desorption profiles during the heat-up ramp of the CO-TPD are nearly identical.

Pre-exponentials and desorption energies determine the mobility of the species. At 150 °C, the accessible thermal energy is  $3.5 \text{ kJ mol}^{-1}$ . Since the adsorption and diffusion energies of all our adsorbates are higher, surface migration is driven by the continuous energy exchange between the adsorbate and substrate. These fluctuations result in random jumps, forming a Markov process [83]. CO is most mobile on Pd and Ru, where the pre-exponential factor is the largest. On Cu, it is bound weakest, meaning that desorption competes with the surface mobility.

Pd and Rh showed one clear desorption peak, suggesting one main type of metal surface sites from which CO desorbed. Pt, Re Ru, and Cu showed two desorption peaks, which suggest that at least two different surface sites are present; however peaks were not clearly separated for Ni. Nevertheless, our model adequately fitted all desorption behavior, taking solely one type of sites into account. Interestingly, the first two catalysts were found to lead to the most varying products (aldehyde group and ring hydrogenation, deoxygenation and in case of Rh/C also ring opening), while the latter follows only one dominant pathway

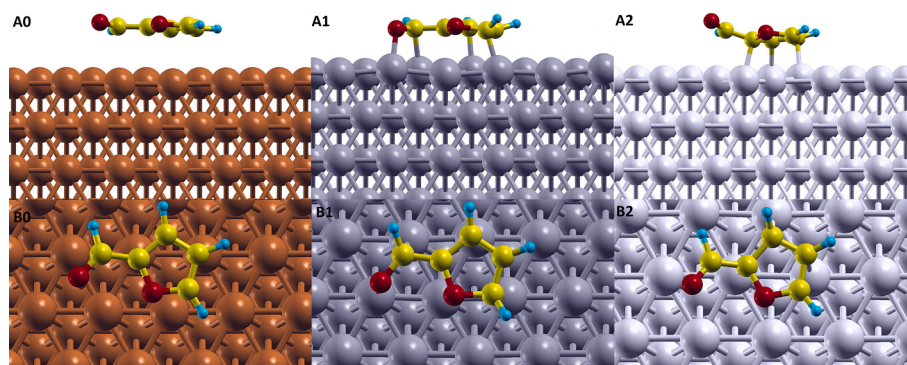


Fig. 2. The adsorption of furfural on 0:Cu, 1:Ni, 2:Pd, where A is the side and B the top view. Colour code: C-yellow, H-cyan, O-red, Cu-orange, Ni-dark purple and Pd-light purple.

through aldehyde group hydrogenation and deoxygenation (see section 3.5. Reaction kinetics and transport phenomena for details).

### 3.5. Reaction kinetics and transport phenomena

#### 3.5.1. Preliminary runs

Preliminary tests were performed to experimentally confirm the absence of the external mass transfer limitations (Run 1 and 2), as no noticeable difference by comparing reaction rates at different stirring speeds was found (Figure S7a and Fig. 5a). Operation in the kinetic regime for all tested catalysts was confirmed, as these tests were performed with the most active Pd/C catalyst. The external mass transfer was therefore sufficiently fast not to affect the global rate even using the catalyst demonstrating the highest TOF. Internal mass transfer limitations also did not play an important role, as the catalyst was used in powder form, therefore the diffusion could easily cope with relatively low global reaction rates (requiring hours for a noticeable conversion). Furthermore, Pd/C was among the catalysts with the smallest average pore diameter (Table 2) and still demonstrated supreme performance, while the pore volume was comparable for all the tested samples ( $0.95 \pm 0.35 \text{ cm}^3 \text{ g}^{-1}$ ). As shown later on, adsorption rate was much faster than surface reaction rates as well.

It was also demonstrated that the support itself has no catalytic activity (Run 3, Figure S7b), proving that the active metal surfaces are solely responsible for the catalytic reactions. The support and its interaction with the metal might however affect the catalytic performance. It was found by Kosydar *et al.* [84] and Mironenko *et al.* [55] that active carbon can even provide additional adsorption sites, while the remaining oxygen-containing functional groups could have an influence on the reaction rates and selectivity. As carbon support was catalytically inactive in absence of the active metal, the effect of the support was neglected in our kinetic modelling. The effect is expected to be rather limited and can also be considered similar across the benchmarked catalysts.

#### 3.5.2. Catalytic activity and modelling results

All catalysts were tested at 100 °C, 150 °C and 200 °C and the data fitted with our micro-kinetic model. The model fits experimental data at all tested temperatures (Figs. 5–7) well for all tested catalysts, although the reaction rate was slightly overestimated in case of Re/C at 100 °C. If the reader is interested in the low concentration products at 150 °C, they are invited to see Supplementary material (Figure S8.). The modelling results show the Pd/C catalyst to be most active at all tested temperatures. The reaction rates were generally at least one order of magnitude higher at 100 °C, compared to the other tested catalysts (Table 5), which is also evident from the total turnover frequency (TOF) values (Table 6). Although the total achieved TOF of Pd/C is also highest at 200 °C, other catalysts become competitive and more selective towards the aldehyde group hydrogenation and deoxygenation. This is also noticeable when

comparing activation energies (Table 5), since the reaction rates with high activation energies are generally dominant at high temperatures. Pt/C, Re/C, Ru/C, and Ni/C showed medium activity, while Rh/C and Cu/C showed to be inferior in the tested temperature range. The lowest activity of Cu can be ascribed to a weak adsorption of furfural and hydrogen to the catalyst surface, as observed in our CO-TPD measurements (low desorption temperature) and theoretical calculations of adsorption energies (Table 3). The final conversion, selectivity and yields for all runs are shown in Table S3. for comparison.

#### 3.5.3. Ring hydrogenation

Pd/C was the only catalyst, which showed ring hydrogenation activity at all tested temperatures, as THFUR was detected and also produced in relatively large quantities even at 100 °C. This is evident from the high reaction rate constant and TOF values for ring hydrogenation reactions (Table 6). The high ring hydrogenation activity could be a result of furfural adsorption orientation with the ring and oxygen tilted away from the surface, as suggested by our theoretical calculations. However, hydrogenation was not selective in terms of various functional groups, as both aldehyde group and ring were hydrogenated with comparable rates at all tested temperatures. Hydrotreatment reactions over Pd/C are not very temperature sensitive due to low activation energies. Nevertheless, faster total hydrogenation and deoxygenation were observed at higher temperatures.

Negligible ring hydrogenation activity was observed with other catalysts up to 150 °C. Ru/C showed mediocre ring saturation activity only at temperatures as high as 200 °C, but was not selective. Rh/C also showed minor ring hydrogenation activity at 200 °C.

#### 3.5.4. Aldehyde group hydrogenation

All tested catalysts exhibited aldehyde group hydrogenation activity. In addition to ring hydrogenation, Pd/C also showed the highest aldehyde group hydrogenation activity at 100 °C, which was more competitive with other catalysts at higher temperatures. All other catalyst showed to be much more selective towards aldehyde group hydrogenation, which is also thermodynamically favorable in comparison to ring hydrogenation (except for Cu), according to potential energy diagrams (Fig. 3). Although Pt/C and Ru/C were less active compared to Pd/C at 100 °C, higher yield towards the aldehyde group hydrogenation product FA was observed. FA was also the main product at 150 °C for most catalysts (Pt/C, Re/C, Ru/C, Rh/C, Ni/C), while the highest yield was obtained by using Ru/C, followed by Re/C and Pt/C. Aldehyde group hydrogenation was faster with all catalysts at 200 °C compared to lower temperatures, although other side or sequential products were observed in all cases, hence lowering the selectivity. Cu/C showed the highest selectivity at 200 °C but is not of a high relevance due to the poor conversion.

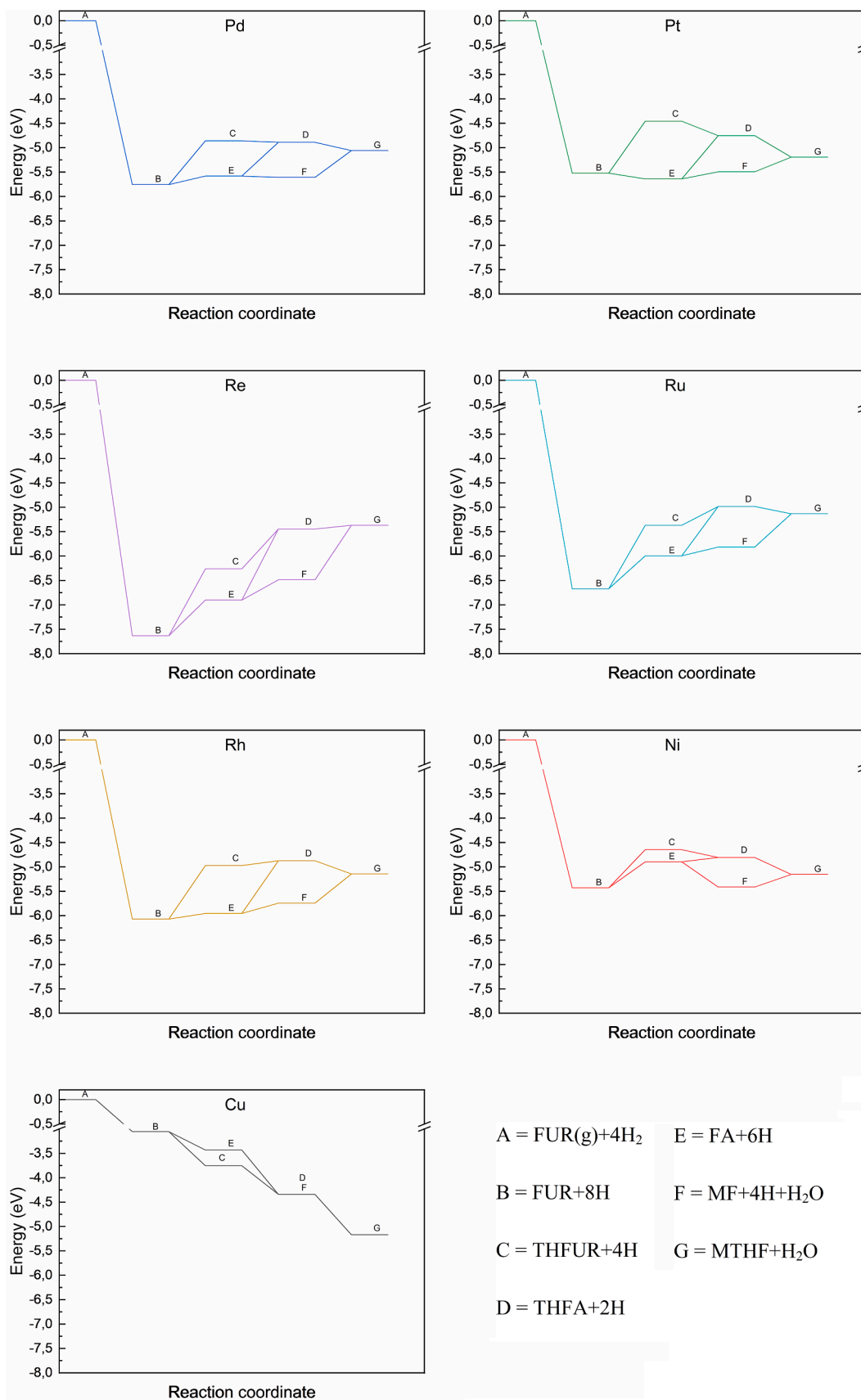


Fig. 3. Potential energy diagrams for all tested active metals.

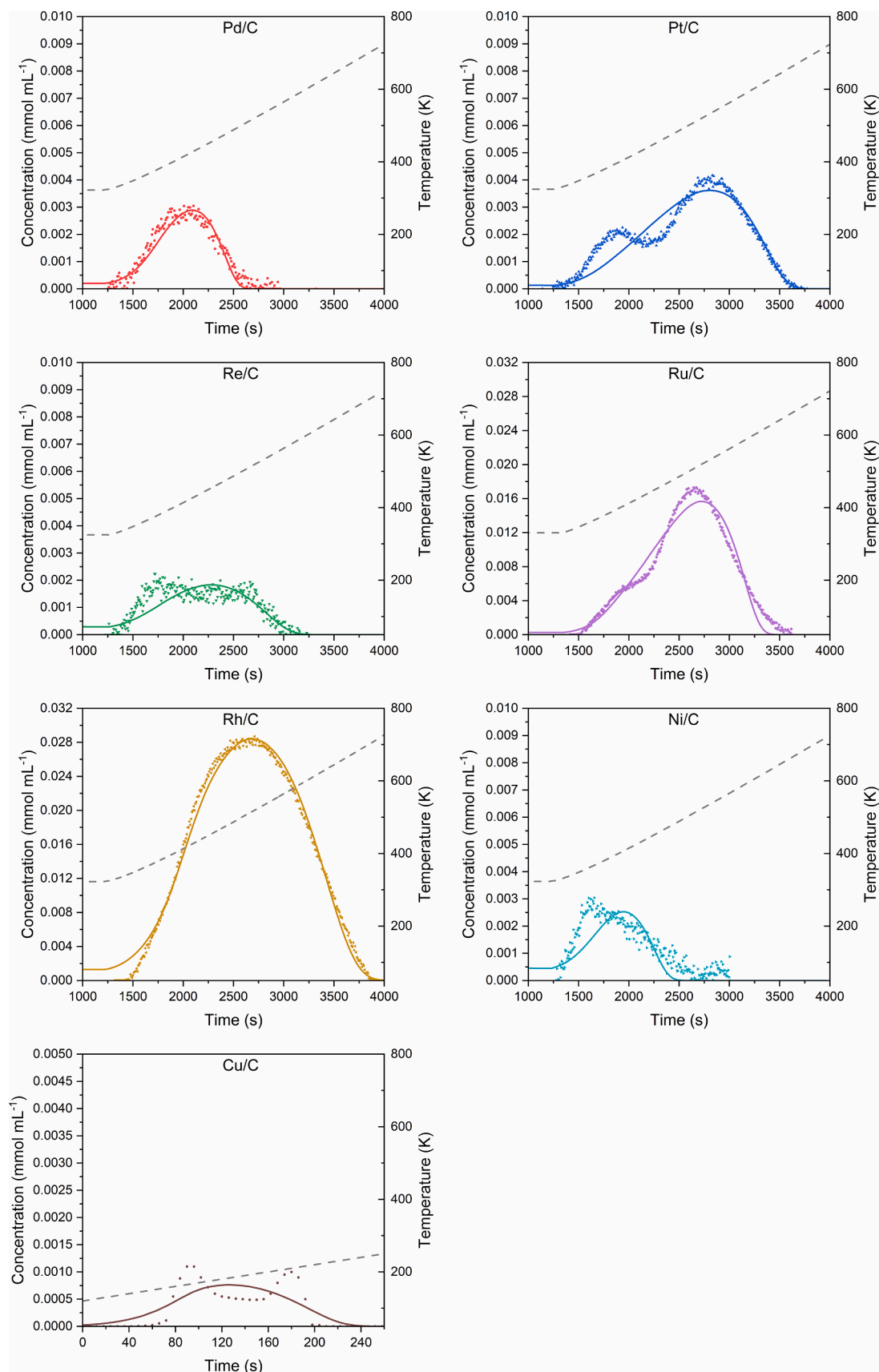


Fig. 4. Experimental (points) and modelled (solid lines) CO-TPD profiles for Pd/C, Pt/C, Re/C, Ru/C, Rh/C, Ni/C and Cu/C, used to obtain kinetic parameters for adsorption and desorption. Dashed line represents the temperature.

**Table 4**

Concentration of surface sites, initial TPD surface coverages and desorption kinetic parameters obtained from CO-TPD.

Parameter	Pd/C	Pt/C	Re/C	Ru/C	Rh/C	Ni/C	Cu/C <sup>a</sup>
$C_{AS}$ [mol $g^{-1}$ ]	4.5 • $10^{-4}$	9.7 • $10^{-4}$	5.6 • $10^{-4}$	3.1 • $10^{-3}$	1.1 • $10^{-2}$	5.5 • $10^{-4}$	8.7 • $10^{-6}$
$\theta_{CO}$	0.77	0.97	0.78	0.96	0.84	0.6	0.74
$k_{des}^b$ [ $s^{-1}$ ]	3.2 • $10^4$	1.1 • $10^3$	1.1 • $10^4$	1.3 • $10^3$	2.3 • $10^3$	6.0 • $10^4$	3.0 • $10^7$
$A_{des}$ [ $s^{-1}$ ]	4.8 • $10^9$	2.7 • $10^8$	3.1 • $10^7$	4.5 • $10^9$	1.4 • $10^7$	8.1 • $10^8$	9.30 • $10^8$
$E_{des}$ [kJ $mol^{-1}$ ]	41.9	43.6	28.0	53.1	30.5	33.4	12.0

a Parameters estimated by fitting literature data [81].

b Desorption rate constant at 150 °C.

### 3.5.5. Deoxygenation

Deoxygenation was found to be slower than hydrogenation of aldehyde group in all cases and was therefore a consecutive reaction after at least one hydrogenation step. A similar trend was observed for both reactions, although higher temperatures were generally needed for deoxygenation to occur. Furfural's aldehyde group hydrogenation, followed by deoxygenation is also the thermodynamically favorable pathway (Fig. 3). No deoxygenation was observed at 100 °C with all catalysts, except for Ru/C being the only catalyst, where the deoxygenation product MF was found in decent quantities. At 200 °C, deoxygenation products were observed with all catalysts but in various quantities. The highest deoxygenation rates at 200 °C were observed with the catalysts exhibiting the highest activation energies for this reaction, such as Pt/C with 125 kJ mol<sup>-1</sup>.

### 3.5.6. Ring hydrogenation, coupled with deoxygenation and ring opening

Higher amounts of MTHF and various ring opening products (Pentane-2-one, butan-1-ol, butane-1,4-diol and pentan-2-ol) were only observed using Rh/C at 200 °C. No such products were found in meaningful concentration at lower temperatures or with any other catalyst. Although some researchers [16] obtained MTHF by using Pd based catalyst and pentanediols by using Pt based catalysts, a different catalyst support or a combination of various catalysts and different solvents (usually 2-propanol or water) were used in those cases. Ma et al. [85] also observed water to play a key role in the ring opening reactions for Pt based catalysts, while only a minor yield of 1.8 % of pentanediols was obtained with THF as solvent and Pt/CeO<sub>2</sub> as catalyst, which explains the lack of such products in our reaction system. The kinetic parameters for these reactions could not be precisely calculated, as higher temperatures would be needed to study them thoroughly. This also results in a less accurate fit of experimental points with modelled data at 200 °C. Nevertheless, 45.3 % MTHF yield was experimentally observed, and it was the only catalyst with ring-opening activity, which makes Rh/C a promising catalyst, worth studying further.

### 3.6. In-silico process optimization and experimental validation

We used the micro-kinetic model and kinetic parameters determined in descriptive phase for predicting the catalytic performance and to optimize the temperature and reaction time, with the goal to obtain the highest yield and selectivity of target products using the most promising catalysts. Temperature and reaction times were optimized for Pd/C, Pt/C, Re/C and Ni/C, which were also experimentally validated at conditions prognosed as optimal. The agreement between modelling forecasts and experimental validation tests is shown in Fig. 8.

Despite Pd/C is promising for producing THFA at higher temperatures and longer reaction times, it seemed to be more interesting for optimizing the yield of THFUR, which was rarely mentioned in the

literature. The optimal selectivity was predicted to be achieved by using very low temperatures. At 40 °C the highest THFUR yield of 48 % was calculated after 437 min of reaction time. The model underestimated the selectivity towards THFUR, as more THFUR was formed in a validation experiment (70 % yield) than expected. Generally, the prediction of high THFUR yield at low temperature was found correct and predicted behavior did not deviate severely, taking into account that the used kinetic parameters are based on catalytic tests performed at significantly higher temperatures (between 100 °C and 200 °C). The process might also be economically favorable, as it could operate nearly at room temperature.

Pt/C catalyst was optimized for MF production. The yield of 95 % (99 % selectivity) was calculated to be achieved at 220 °C by prolonging the reaction time to 930 min. Deoxygenation was slightly faster than expected and also up to 12 % of ring opening products were observed at the end of reaction. This was not predicted in our model, as ring opening products were not observed below 200 °C during shorter catalytic tests. An experimental yield of 81 % was achieved after 1080 min and 85 % after 1320 min, which is a reasonably good agreement with *in silico* prediction.

Re/C was expected to be suitable for FA production. By prolonging the reaction time to 1040 min at 135 °C, a targeted 78 % yield with 84 % selectivity should be achieved. A maximum yield of 49 % was achieved experimentally only after 1330 min. Additionally, two separate runs at same experimental conditions were performed with Re/C catalyst. Combined experimental points are shown in Fig. 8 to confirm good repeatability.

Ni was also promising for FA production as a cheaper alternative. The optimal conditions were found at 212 °C after 345 min reaction time. We achieved a good fit for aldehyde group hydrogenation (as seen from furfural consumption). However, faster hydrodeoxygenation was observed experimentally, as the test was performed 12 °C above our prior catalytic tests. The obtained parameters for reaction  $k_5$  seem to be slightly underestimated, as MF was detected only at 150 °C and 200 °C in lower concentrations. We believe this phenomenon to be a result thermodynamics, as a highly exothermic FA deoxygenation reaction (Fig. 3) was only observed with Ni metal (in addition to Cu, which was mostly inactive), once the reaction barrier was overcome. Nevertheless, the experimental results suggest Ni/C to be the best catalyst for MF production at 212 °C, as up to 95 % yield could be experimentally achieved after only 346 min of reaction. A higher yield could be obtained in a much shorter time and at slightly lower temperature, compared with Pt/C.

Overall, the model suggested optimized conditions well, especially by taking into account that all optimization experiments were validated out of our prior experimental temperature and/or reaction time range. Only the deoxygenation rate ( $k_5$ ) was found not to be valid above 200 °C with Ni/C.

## 4. Conclusion

Seven different metals, dispersed on activated carbon (Pd/C, Pt/C, Re/C, Ru/C, Rh/C, Ni/C and Cu/C), have been tested for their activity in hydrotreatment of furfural. The catalysts were tested at three different temperatures (100 °C, 150 °C, and 200 °C) with tetrahydrofuran (THF) as a solvent. Initial testing revealed that mass transfer limitations did not play a role in the reaction. Consequently, the observed reactions were governed by the intrinsic reactivity of the catalyst. Temperature programmed desorption (TPD) with CO was used to measure the amount of active sites. A plug-flow reactor model was constructed and parameterized to model the adsorption and desorption of CO in the experiment. By fitting the experimental TPD plots to the model, the concentration of active sites, the adsorption interaction and its rate constants were obtained, which were used in the micro-kinetic model describing the conversion of furfural.

To describe the performance of the catalysts with respect to activity

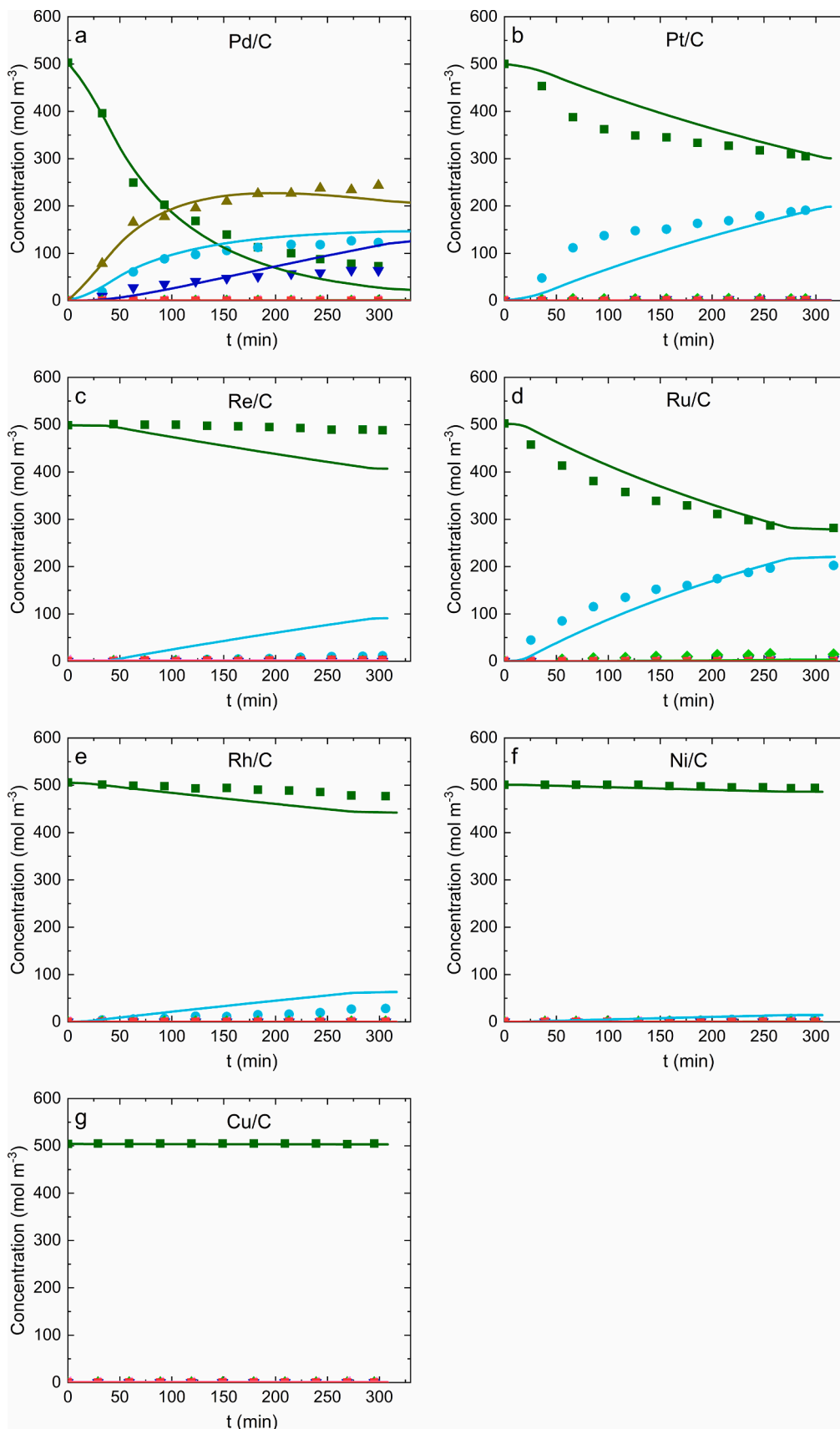
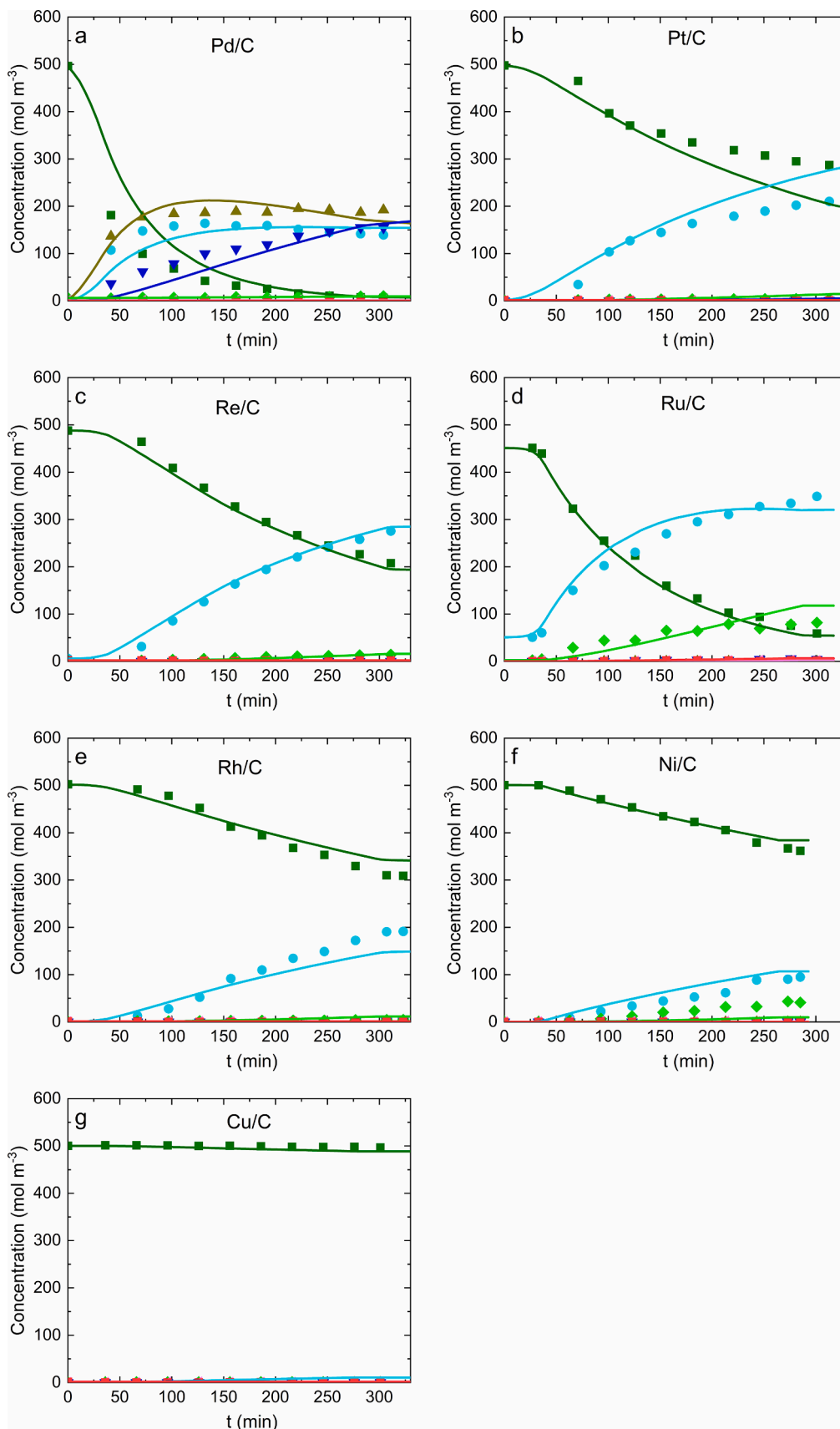


Fig. 5. Furfural hydrotreatment at 100 °C by using 0.2 wt% of Pd/C, Pt/C, Re/C, Ru/C, Rh/C, Ni/C or Cu/C catalysts, 5 wt% of furfural, 94.8 wt% of tetrahydrofuran and 60 bar of pure hydrogen. ■ FUR, ● FA, ▲ THFUR, ▼ THFA, ● MF, ■ MTHF, ■ OR.



**Fig. 6.** Furfural hydrotreatment at 150 °C by using 0.2 wt% of Pd/C, Pt/C, Re/C, Ru/C, Rh/C, Ni/C or Cu/C catalysts, 5 wt% of furfural, 94.8 wt% of tetrahydrofuran and 60 bar of pure hydrogen. ■ FUR, ● FA, ▲ THFUR, ▼ THFA, ◆ MF, ■ MTHF, ■ OR.

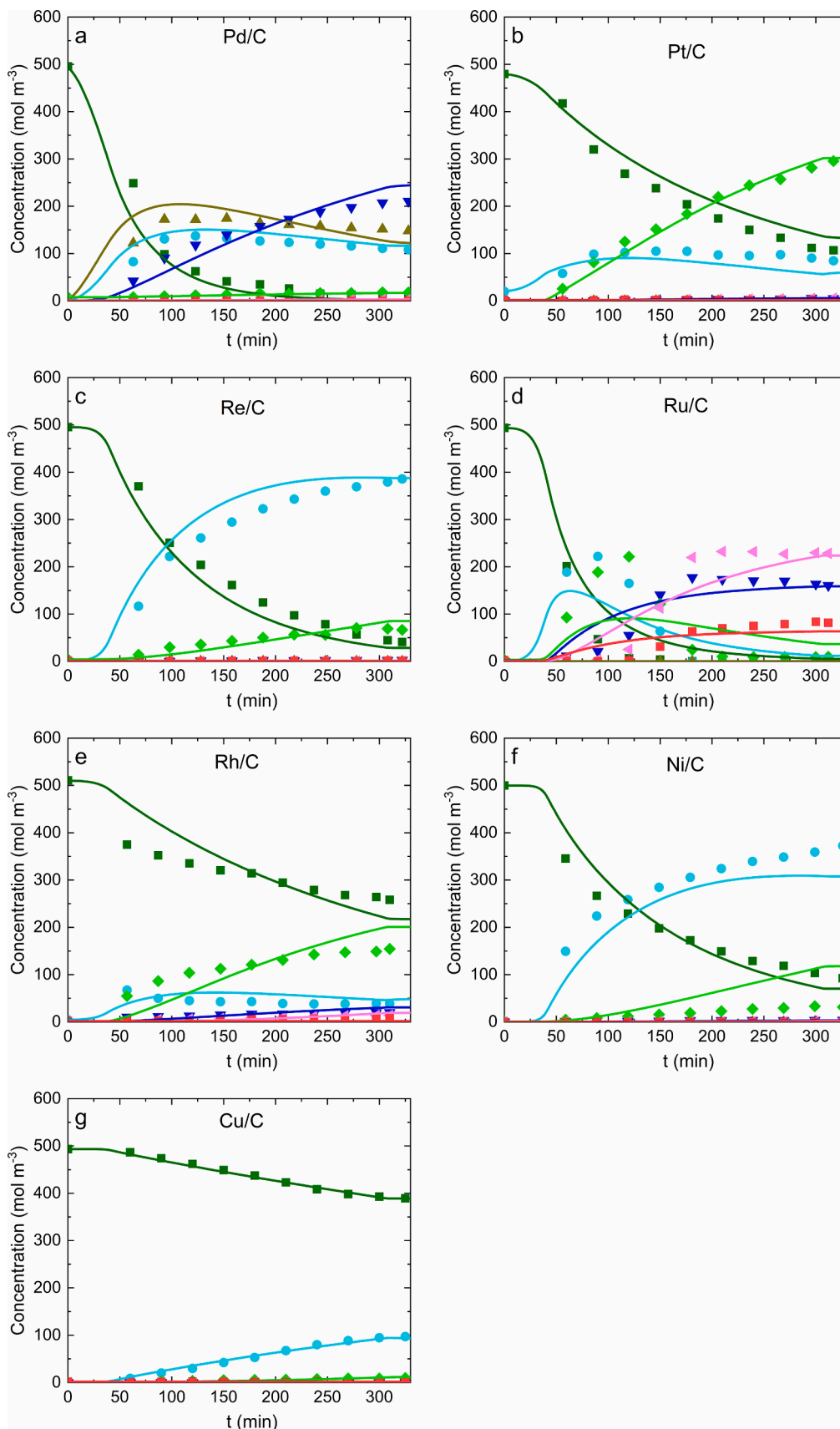


Fig. 7. Furfural hydrotreatment at 200 °C by using 0.2 wt% of Pd/C, Pt/C, Re/C, Ru/C, Rh/C, Ni/C or Cu/C catalysts, 5 wt% of furfural, 94.8 wt% of tetrahydrofuran and 60 bar of pure hydrogen. ■ FUR, ● FA, ▲ THFUR, ▼ THFA, ◆ MF, ▲ MTHF, ■ OR.

**Table 5**  
Surface kinetics parameters determined by the regression analysis.

i	Pd/C	Pt/C	Re/C	Ru/C	Rh/C	Ni/C	Cu/C
Reaction rate constants ( $k_i$ ) at 100 °C [ $s^{-1}$ ]							
1	$(3.9 \pm 0.2) \cdot 10^1$	$7.7 \pm 0.4$	$5.9 \pm 0.2$	$3.0 \pm 0.5$	$(2.0 \pm 0.1) \cdot 10^{-1}$	$(8.7 \pm 0.3) \cdot 10^{-1}$	$(2.56 \pm 0.05) \cdot 10^{-2}$
2	$(7.8 \pm 0.5) \cdot 10^1$	0	0	0	0	0	0
3	$(2 \pm 2) \cdot 10^1$	0	0	0	0	0	0
4	$1.7 \pm 0.8$	$(1 \pm 1) \cdot 10^{-1}$	0	$(4 \pm 4) \cdot 10^{-5}$	$(2 \pm 4) \cdot 10^{-4}$	$(4 \pm 4) \cdot 10^{-7}$	
5	$(3 \pm 3) \cdot 10^{-1}$	$(8 \pm 2) \cdot 10^{-3}$	$(6 \pm 1) \cdot 10^{-1}$	$(1.3 \pm 0.3) \cdot 10^{-1}$	$(3 \pm 1) \cdot 10^{-3}$	$2 \pm 4$	$1.7 \pm 0.1$
6	0	0	0	0	0	0	0
7	$(2 \pm 2) \cdot 10^{-1}$	0	0	$(1.1 \pm 0.6) \cdot 10^{-3}$	$(6 \pm 6) \cdot 10^{-4}$	$(1 \pm 1) \cdot 10^{-3}$	0
8	0	0	0	$(1 \pm 1) \cdot 10^{-3}$	$(1 \pm 1) \cdot 10^{-6}$	$(1 \pm 1) \cdot 10^{-3}$	0
Activation energy ( $E_{a_i}$ ) [kJ mol <sup>-1</sup> ]							
1	$6.3 \pm 0.6$	$6 \pm 1$	$30.3 \pm 0.6$	$27 \pm 2$	$18.8 \pm 0.8$	$57.1 \pm 0.9$	$63.66 \pm 0.03$
2	$1.2 \pm 0.9$	n.a.	n.a.	n.a.	n.a.	n.a.	n.a.
3	$0.7 \pm 0.7$	n.a.	n.a.	n.a.	n.a.	n.a.	n.a.
4	$30 \pm 1$	$27 \pm 5$	n.a.	$178 \pm 30$	$116 \pm 26$	$205 \pm 16$	n.a.
5	$31 \pm 1$	$125 \pm 2$	$29 \pm 2$	$68 \pm 7$	$106 \pm 30$	$28 \pm 3$	$0.02 \pm 0.02$
6	n.a.	n.a.	n.a.	n.a.	n.a.	n.a.	n.a.
7	$47 \pm 20$	n.a.	n.a.	$140 \pm 8$	$83 \pm 80$	$95 \pm 13$	n.a.
8	n.a.	n.a.	n.a.	$117 \pm 7$	$50 \pm 50$	$12 \pm 12$	n.a.

**Table 6**  
Maximum TOF with 95 % confidence intervals for each reaction step, calculated during experimental runs at 100 °C and 200 °C.

i	Pd/C	Pt/C	Re/C	Ru/C	Rh/C	Ni/C	Cu/C
TOF <sub>i</sub> at 100 °C [ $s^{-1}$ ]							
1	$(3.3 \pm 0.2) \cdot 10^{-2}$	$(6.8 \pm 0.4) \cdot 10^{-3}$	$(6.7 \pm 0.3) \cdot 10^{-3}$	$(8 \pm 1) \cdot 10^{-4}$	$(5.1 \pm 0.4) \cdot 10^{-5}$	$(1.12 \pm 0.04) \cdot 10^{-3}$	$((3.22 \pm 0.06) \cdot 10^{-5})$
2	$(6.7 \pm 0.3) \cdot 10^{-2}$	0	0	0	0	0	0
3	$(8 \pm 7) \cdot 10^{-3}$	0	0	0	0	0	0
4	$(3 \pm 1) \cdot 10^{-4}$	$(8 \pm 8) \cdot 10^{-5}$	0	0	$(4 \pm 4) \cdot 10^{-9}$	$(2 \pm 2) \cdot 10^{-6}$	
5	$(9 \pm 9) \cdot 10^{-5}$	$(2 \pm 0.7) \cdot 10^{-6}$	$(1.2 \pm 0.3) \cdot 10^{-4}$	$(4 \pm 1) \cdot 10^{-6}$	$(2 \pm 1) \cdot 10^{-8}$	$(5.2 \pm 0.1) \cdot 10^{-5}$	$(2.9 \pm 0.3) \cdot 10^{-6}$
6	0	0	0	0	0	0	0
7	$(3 \pm 3) \cdot 10^{-6}$	0	0	$(1.1 \pm 0.9) \cdot 10^{-10}$	$(2 \pm 2) \cdot 10^{-12}$	$(2 \pm 2) \cdot 10^{-8}$	0
8	0	0	0	$(1 \pm 1) \cdot 10^{-7}$	$(1 \pm 1) \cdot 10^{-7}$	$(2 \pm 2) \cdot 10^{-7}$	0
Total*	$(6.7 \pm 0.3) \cdot 10^{-2}$	$(6.8 \pm 0.4) \cdot 10^{-3}$	$(6.7 \pm 0.3) \cdot 10^{-3}$	$(8 \pm 1) \cdot 10^{-4}$	$(5.1 \pm 0.4) \cdot 10^{-5}$	$(1.12 \pm 0.04) \cdot 10^{-3}$	$(3.22 \pm 0.06) \cdot 10^{-5}$
TOF <sub>i</sub> at 200 °C [ $s^{-1}$ ]							
1	$(5.3 \pm 0.3) \cdot 10^{-2}$	$(1.8 \pm 0.2) \cdot 10^{-2}$	$(6.9 \pm 0.5) \cdot 10^{-2}$	$(2.7 \pm 0.6) \cdot 10^{-2}$	$(1.18 \pm 0.01) \cdot 10^{-2}$	$(6.9 \pm 0.5) \cdot 10^{-2}$	$(3.51 \pm 0.07) \cdot 10^{-3}$
2	$(7.6 \pm 0.7) \cdot 10^{-2}$	0	0	0	0	0	0
3	$(1 \pm 1) \cdot 10^{-2}$	0	0	0	0	0	0
4	$(3.5 \pm 0.9) \cdot 10^{-3}$	$(5 \pm 5) \cdot 10^{-4}$	0	0	$(3 \pm 3) \cdot 10^{-4}$	$(4 \pm 4) \cdot 10^{-2}$	
5	$(10 \pm 10) \cdot 10^{-4}$	$(1.0 \pm 0.2) \cdot 10^{-2}$	$(4 \pm 1) \cdot 10^{-3}$	$(6.2 \pm 0.4) \cdot 10^{-3}$	$(7 \pm 6) \cdot 10^{-4}$	$(4 \pm 4) \cdot 10^{-3}$	$(4.2 \pm 0.4) \cdot 10^{-4}$
6	0	0	0	0	0	0	0
7	$(2 \pm 2) \cdot 10^{-3}$	0	0	$(2.7 \pm 0.4) \cdot 10^{-3}$	$(7 \pm 7) \cdot 10^{-4}$	$(3 \pm 3) \cdot 10^{-5}$	0
8	0	0	0	$(5 \pm 5) \cdot 10^{-3}$	$(3 \pm 3) \cdot 10^{-4}$	$(2 \pm 2) \cdot 10^{-7}$	0
Total*	$(7.6 \pm 0.7) \cdot 10^{-2}$	$(1.7 \pm 0.2) \cdot 10^{-2}$	$(6.9 \pm 0.5) \cdot 10^{-2}$	$(4 \pm 2) \cdot 10^{-2}$	$(1.27 \pm 0.2) \cdot 10^{-3}$	$(6.9 \pm 0.5) \cdot 10^{-2}$	$(3.51 \pm 0.07) \cdot 10^{-3}$

\*Highest obtained cumulative TOF during the reaction.

and selectivity at different operating conditions, a generalized microkinetic model was developed. It is valid for all studied catalysts at all tested conditions.

Pd/C consistently showed the highest activity regardless of the conditions. However, the catalyst was poorly selective, hydrogenating both the aromatic ring and the aldehyde group, eventually yielding fully hydrogenated THFA. The temperature did not have a strong effect on the selectivity, although ring hydrogenation was slightly favored at lower temperature, while higher temperature promoted full hydrogenation. Pd/C was the only catalyst with ring hydrogenation activity at 100 °C and 150 °C, which makes it the best candidate for tetrahydrofurfural and tetrahydrofurfuryl alcohol production. Pt/C and Ru/C had moderate activity at 100 °C, selectively producing furfuryl alcohol, while Ru/C also showed minor deoxygenation activity. Furfuryl alcohol was also observed in low concentration with Re/C and Rh/C, as well. Copper was the least active catalyst, inert up to 150 °C. Pt/C, Re/C, Rh/C, Ru/C and

Ni/C all exhibited selective aldehyde group hydrogenation at 150 °C (to FA), followed by deoxygenation at higher temperatures (to MF). More noticeable deoxygenation at 150 °C was observed with Ru/C and Ni/C. At higher temperatures (200 °C), the difference in activity between Pd/C and other catalysts was less pronounced. In addition to aldehyde group hydrogenation, all catalysts showed some deoxygenation ability.

For additional insight in the reaction mechanism, DFT calculations were employed. The investigated catalysts were modelled as extended metallic surface, omitting the support effect (since C is rather inert). Despite known limitations of the study (extended monometallic surfaces, no support), some trends that help explain experimental data were discovered. It was found that on all catalysts except Cu, the hydro (deoxy)genation of the side group is more thermodynamically favorable than ring hydrogenation. This means that FA and MF preferentially form, which was confirmed experimentally. We show that Pd and Pt have the unique combination of strong adsorption energies and

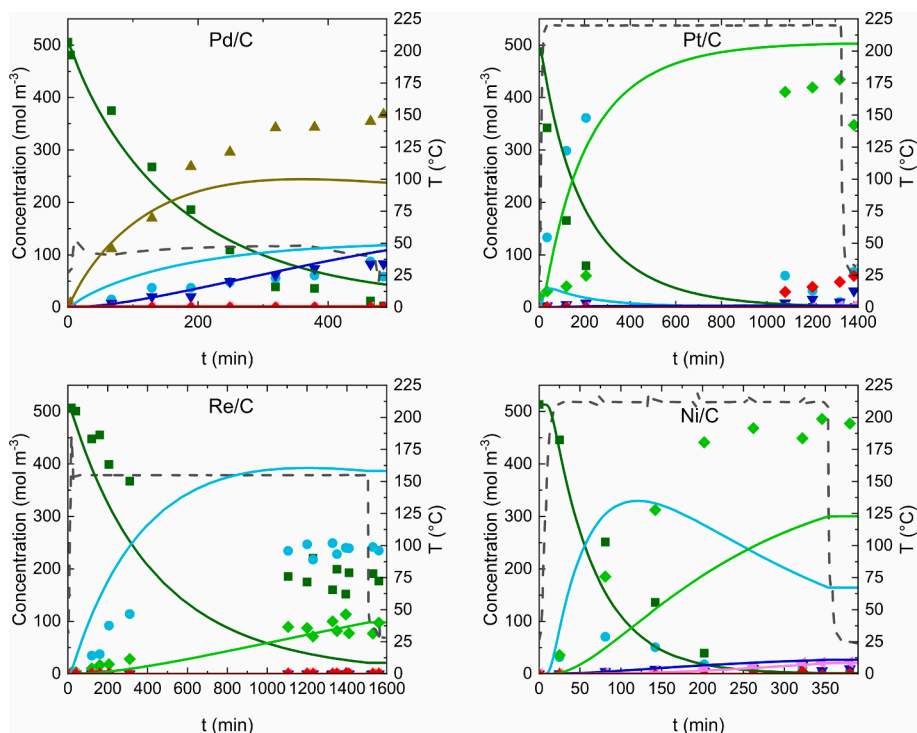


**Fig. 8.** Optimization and validation runs at optimized temperature and reaction time, by using 0.2 wt% of Pd/C, Pt/C, Re/C, and Ni/C, 5 wt% of furfural, 94.8 wt% of tetrahydrofuran and 60 bar of pure hydrogen. ■ FUR, ● FA, ▲ THFUR, ▼ THFA, ◆ MF, ■ MTHF, ● OR.

exothermic (or only slightly endothermic) reaction steps, explaining their superb performance.

Ultimately, the microkinetic model was used as a predictive tool to optimize the operating conditions for the best performing catalysts. Among them, Pd/C showed high ring hydrogenation activity even at 40 °C, obtaining up to 85 % yield of tetrahydrofurfural. Ni/C was showed to be highly active and selective at 212 °C. A 95 % yield of 2-methylfuran was experimentally achieved at 212 °C, while furfuryl alcohol was the main product at lower temperatures. Re/C was selective to furfuryl alcohol at all temperatures.

#### Declaration of Competing Interest

The authors declare that they have no known competing financial interests or personal relationships that could have appeared to influence the work reported in this paper.

#### Acknowledgements

This research was funded by the Slovenian Research Agency (basic post-doctoral research project Z2-9200 (M.G.), research project J1-3020 (M.H.), research core funding P2-0152 (B.L.), P1-0418 (M.G.), P2-0421 (M.H.), and infrastructure funding I0-0039 (M.H.)). The work was partially carried out within the RDI project Cel. Cycle: »Potential of biomass for development of advanced materials and bio-based products«, which is co-financed by the Republic of Slovenia, Ministry of Education, Science and Sport, and the European Union through the European Regional Development Fund, 2016-2020.

#### Appendix A. Supplementary data

Supplementary data to this article can be found online at <https://doi.org/10.1016/j.cej.2022.135070>.

[org/10.1016/j.cej.2022.135070](https://doi.org/10.1016/j.cej.2022.135070).

#### References

- [1] X. Li, P. Jia, T. Wang, Furfural: a promising platform compound for sustainable production of C<sub>4</sub> and C<sub>5</sub> chemicals, *ACS Catal.* 6 (11) (2016) 7621–7640, <https://doi.org/10.1021/acscatal.6b01838>.
- [2] K. Dussan, B. Girisuta, D. Haverty, J.J. Leahy, M.H.B. Hayes, Kinetics of levulinic acid and furfural production from *Miscanthus × giganteus*, *Bioresour. Technol.* 149 (2013) 216–224, <https://doi.org/10.1016/j.biortech.2013.09.006>.
- [3] D.M. Alonso, J.Q. Bond, J.A. Dumesic, Catalytic conversion of biomass to biofuels, *Green Chem.* 12 (9) (2010) 1493, <https://doi.org/10.1039/c004654j>.
- [4] M. Dashtban, A. Gilbert, P. Feteihi, Production of Furfural: Overview and Challenges, *J. Sci. Technol. For. Prod. Process.* 2 (2012) 44–53.
- [5] T. Wery, G. Petersen, Top Value Added Chemicals from Biomass: Volume I—Results of Screening for Potential Candidates from Sugars and Synthesis Gas, U.S. Dep. Energy, 2004. <https://doi.org/10.2172/15008859>.
- [6] J.J. Bozell, G.R. Petersen, Technology development for the production of biobased products from biorefinery carbohydrates—the US Department of Energy’s “Top 10” revisited, *Green Chem.* 12 (2010) 539–554, <https://doi.org/10.1039/b922014c>.
- [7] L.T. Mika, E. Cséfalvay, Á. Németh, Catalytic Conversion of Carbohydrates to Initial Platform Chemicals: Chemistry and Sustainability, *Chem. Rev.* 118 (2) (2018) 505–613, <https://doi.org/10.1021/acs.chemrev.7b00395>.
- [8] J. Chheda, G. Huber, J. Dumesic, Liquid-Phase Catalytic Processing of Biomass-Derived Oxygenated Hydrocarbons to Fuels and Chemicals, *Angew. Chem., Int. Ed.* 46 (38) (2007) 7164–7183, <https://doi.org/10.1002/anie.200604274>.
- [9] M. Besson, P. Gallezot, C. Pinel, Conversion of Biomass into Chemicals over Metal Catalysts, *Chem. Rev.* 114 (3) (2014) 1827–1870, <https://doi.org/10.1021/cr4002269>.
- [10] M.J. Climent, A. Corma, S. Iborra, Conversion of biomass platform molecules into fuel additives and liquid hydrocarbon fuels, *Green Chem.* 16 (2014) 516–547, <https://doi.org/10.1039/c3gc41492b>.
- [11] R. Mariscal, P. Maireles-Torres, M. Ojeda, I. Sádaba, M. López Granados, Furfural: a renewable and versatile platform molecule for the synthesis of chemicals and fuels, *Energy Environ. Sci.* 9 (4) (2016) 1144–1189.
- [12] G. Machado, S. Leon, F. Santos, R. Lourega, J. Dullius, M.E. Mollmann, P. Eichler, Literature Review on Furfural Production from Lignocellulosic Biomass, *Nat. Resour.* 07 (03) (2016) 115–129, <https://doi.org/10.4236/nr.2016.73012>.
- [13] A.E. Eseyin, P.H. Steele, An overview of the applications of furfural and its derivatives, *Int. J. Adv. Chem.* 3 (2015) 42, <https://doi.org/10.14419/ijac.v3i2.5048>.

- [14] Y. Wang, D. Zhao, D. Rodríguez-Padrón, C. Len, Recent advances in catalytic hydrogenation of furfural, *Catalysts*. 9 (10) (2019) 796, <https://doi.org/10.3390/catal9100796>.
- [15] K. Gupta, R.K. Rai, S.K. Singh, Metal Catalysts for the Efficient Transformation of Biomass-derived HMF and Furfural to Value Added Chemicals, *ChemCatChem* 10 (11) (2018) 2326–2349, <https://doi.org/10.1002/cctc.201701754>.
- [16] S. Chen, R. Wojcieszak, F. Dumeignil, E. Marceau, S. Royer, How Catalysts and Experimental Conditions Determine the Selective Hydroconversion of Furfural and 5-Hydroxymethylfurfural, *Chem. Rev.* 118 (22) (2018) 11023–11117, <https://doi.org/10.1021/acs.chemrev.8b00134>.
- [17] S. Sittitha, D.E. Resasco, Hydrodeoxygenation of Furfural Over Supported Metal Catalysts: A Comparative Study of Cu, Pd and Ni, *Catal. Lett.* 141 (6) (2011) 784–791, <https://doi.org/10.1007/s10562-011-0581-7>.
- [18] Y. Wang, P. Prinsen, K.S. Triantafyllidis, S.A. Karakoulia, P.N. Trikalitis, A. Yezec, C. Len, R. Luque, A. Yezec, C. Len, R. Luque, Comparative Study of Supported Monometallic Catalysts in the Liquid-Phase Hydrogenation of Furfural: Batch Versus Continuous Flow, *ACS Sustain. Chem. Eng.* 6 (2018) 9831–9844, <https://doi.org/10.1021/acsschemeng.8b00984>.
- [19] B. Chen, F. Li, Z. Huang, G. Yuan, Tuning catalytic selectivity of liquid-phase hydrogenation of furfural via synergistic effects of supported bimetallic catalysts, *Appl. Catal., A*. 500 (2015) 23–29, <https://doi.org/10.1016/j.apcata.2015.05.006>.
- [20] Y. Nakagawa, K. Tomishige, Total hydrogenation of furan derivatives over silica-supported Ni-Pd alloy catalyst, *Catal. Commun.* 12 (3) (2010) 154–156, <https://doi.org/10.1016/j.catcom.2010.09.003>.
- [21] Y. Nakagawa, H. Nakazawa, H. Watanabe, K. Tomishige, Total Hydrogenation of Furfural over a Silica-Supported Nickel Catalyst Prepared by the Reduction of a Nickel Nitrate Precursor, *ChemCatChem* 4 (11) (2012) 1791–1797, <https://doi.org/10.1002/cctc.201200218>.
- [22] M. Manikandan, A.K. Venugopal, K. Prabu, R.K. Jha, R. Thirumalaiswamy, Role of surface synergistic effect on the performance of Ni-based hydrotalcite catalyst for highly efficient hydrogenation of furfural, *J. Mol. Catal. A Chem.* 417 (2016) 153–162, <https://doi.org/10.1016/j.molcata.2016.03.019>.
- [23] T.V. Kotbagi, H.R. Gurav, A.S. Nagpure, S.V. Chilukuri, M.G. Bakker, Highly efficient nitrogen-doped hierarchically porous carbon supported Ni nanoparticles for the selective hydrogenation of furfural to furfuryl alcohol, *RSC Adv.* 6 (72) (2016) 67662–67668.
- [24] M.-Y. Chen, C.-B. Chen, B. Zada, Y. Fu, Perovskite type oxide-supported Ni catalysts for the production of 2,5-dimethylfuran from biomass-derived 5-hydroxymethylfurfural, *Green Chem.* 18 (13) (2016) 3858–3866.
- [25] L. Liu, H. Lou, M. Chen, Selective hydrogenation of furfural to tetrahydrofurfuryl alcohol over Ni/CNTs and bimetallic Cu[*sbnd*]Ni/CNTs catalysts, *Int. J. Hydrogen Energy*. 41 (2016) 14721–14731, <https://doi.org/10.1016/j.ijhydene.2016.05.188>.
- [26] J. Wu, G. Gao, J. Li, P. Sun, X. Long, F. Li, Efficient and versatile CuNi alloy nanocatalysts for the highly selective hydrogenation of furfural, *Appl. Catal., B*. 203 (2017) 227–236, <https://doi.org/10.1016/j.apcatb.2016.10.038>.
- [27] S.H. Pang, N.E. Love, J.W. Medlin, Synergistic effects of alloying and thiolate modification in furfural hydrogenation over Cu-based catalysts, *J. Phys. Chem. Lett.* 5 (23) (2014) 4110–4114, <https://doi.org/10.1021/jz502153q>.
- [28] Y. Song, W. Li, M. Zhang, K. Tao, Hydrogenation of furfuryl alcohol to tetrahydrofurfuryl alcohol on NiB/SiO<sub>2</sub> amorphous alloy catalyst, *Front. Chem. Eng. China*. 1 (2) (2007) 151–154, <https://doi.org/10.1007/s11705-007-0028-2>.
- [29] Y. Nakagawa, M. Tamura, K. Tomishige, Catalytic Reduction of Biomass-Derived Furanic Compounds with Hydrogen, *ACS Catal.* 3 (12) (2013) 2655–2668, <https://doi.org/10.1021/cs400616p>.
- [30] V. Vorotnikov, G. Mpourmpakis, D.G. Vlachos, DFT Study of Furfural Conversion to Furan, Furfuryl Alcohol, and 2-Methylfuran on Pd(111), *ACS Catal.* 2 (12) (2012) 2496–2504, <https://doi.org/10.1021/cs300395a>.
- [31] S.H. Pang, J.W. Medlin, Adsorption and Reaction of Furfural and Furfuryl Alcohol on Pd(111): Unique Reaction Pathways for Multifunctional Reagents, *ACS Catal.* 1 (10) (2011) 1272–1283, <https://doi.org/10.1021/cs200226h>.
- [32] R. Šivec, B. Likozar, M. Grlic, Surface kinetics and transport phenomena modelling for furfural hydrotreatment over Pd/C in isopropanol and tetrahydrofuran, *Appl. Surf. Sci.* 541 (2021) 148485, <https://doi.org/10.1016/j.apsusc.2020.148485>.
- [33] C. Li, G. Xu, X. Liu, Y. Zhang, Y. Fu, Hydrogenation of Biomass-Derived Furfural to Tetrahydrofurfuryl Alcohol over Hydroxyapatite-Supported Pd Catalyst under Mild Conditions, *Ind. Eng. Chem. Res.* 56 (31) (2017) 8843–8849, <https://doi.org/10.1021/acs.iecr.7b02046>.
- [34] S.M. Rogers, C.R.A. Catlow, C.E. Chan-Thaw, A. Chutia, N. Jian, R.E. Palmer, M. Perdjón, A. Thetford, N. Dimitratos, A. Villa, P.P. Wells, Tandem Site- and Size-Controlled Pd Nanoparticles for the Directed Hydrogenation of Furfural, *ACS Catal.* 7 (4) (2017) 2266–2274, <https://doi.org/10.1021/acscatal.6b0319010.1021/acscatal.6b03190.s001>.
- [35] S. Bhogesararao, D. Srinivas, Catalytic conversion of furfural to industrial chemicals over supported Pt and Pd catalysts, *J. Catal.* 327 (2015) 65–77, <https://doi.org/10.1016/j.jcat.2015.04.018>.
- [36] N.S. Biradar, A.M. Hengne, S.N. Birajdar, P.S. Niphadkar, P.N. Joshi, C.V. Rode, Single-pot formation of THFAL via catalytic hydrogenation of FFR over Pd/MFI catalyst, *ACS Sustain. Chem. Eng.* 2 (2) (2014) 272–281, <https://doi.org/10.1021/sc400302b>.
- [37] L.-J. Liu, H.-M. Guo, B.o. Xue, H. Lou, M. Chen, Hydrogenation in supercritical conditions catalyzed by palladium supported on modified activated carbon, *RSC Adv.* 5 (82) (2015) 66704–66710.
- [38] R. Albilali, M. Douthwaite, Q. He, S.H. Taylor, The selective hydrogenation of furfural over supported palladium nanoparticle catalysts prepared by sol-immobilisation: Effect of catalyst support and reaction conditions, *Catal. Sci. Technol.* 8 (1) (2018) 252–267.
- [39] S.H. Pang, C.A. Schoenbaum, D.K. Schwartz, J.W. Medlin, J. Will Medlin, Effects of Thiol Modifiers on the Kinetics of Furfural Hydrogenation over Pd Catalysts, *ACS Catal.* 4 (2014) 3123–3131, <https://doi.org/10.1021/cs500598y>.
- [40] Y. Nakagawa, K. Takada, M. Tamura, K. Tomishige, Total Hydrogenation of Furfural and 5-Hydroxymethylfurfural over Supported Pd–Ir Alloy Catalyst, *ACS Catal.* 4 (8) (2014) 2718–2726, <https://doi.org/10.1021/cs500620b>.
- [41] M.J. Taylor, L.i. Jiang, J. Reichert, A.C. Papageorgiou, S.K. Beaumont, K. Wilson, A.F. Lee, J.V. Barth, G. Kyriakou, Catalytic Hydrogenation and Hydrodeoxygenation of Furfural over Pt(111): A Model System for the Rational Design and Operation of Practical Biomass Conversion Catalysts, *J. Phys. Chem. C*. 121 (15) (2017) 8490–8497, <https://doi.org/10.1021/acs.jpcc.7b01744>.
- [42] C. Wang, J. Luo, V. Liao, J.D. Lee, T.M. Onn, C.B. Murray, R.J. Gorte, A comparison of furfural hydrodeoxygenation over Pt-Co and Ni-Fe catalysts at high and low H<sub>2</sub> pressures, *Catal. Today*. 302 (2018) 73–79, <https://doi.org/10.1016/j.cattod.2017.06.042>.
- [43] X. Liu, B. Zhang, B. Fei, X. Chen, J. Zhang, X. Mu, Tunable and selective hydrogenation of furfural to furfuryl alcohol and cyclopentanone over Pt supported on biomass-derived porous heteroatom doped carbon, *Faraday Discuss.* 202 (2017) 79–98, <https://doi.org/10.1039/c7fd00041c>.
- [44] M.G. Dohade, P.L. Dhepe, Efficient hydrogenation of concentrated aqueous furfural solutions into furfuryl alcohol under ambient conditions in presence of PtCo bimetallic catalyst, *Green Chem.* 19 (4) (2017) 1144–1154.
- [45] J. Llop Castelbou, K.C. Szeto, W. Barakat, N. Merle, C. Godard, M. Taoufik, C. Claver, A new approach for the preparation of well-defined Rh and Pt nanoparticles stabilized by phosphine-functionalized silica for selective hydrogenation reactions, *Chem. Commun.* 53 (22) (2017) 3261–3264.
- [46] M. Chatterjee, A. Chatterjee, T. Ishizaka, H. Kawanami, Defining Pt-compressed CO<sub>2</sub> synergy for selectivity control of furfural hydrogenation, *RSC Adv.* 8 (36) (2018) 20190–20201.
- [47] Á. O’Driscoll, J.J. Leahy, T. Curtin, Curtin, The influence of metal selection on catalyst activity for the liquid phase hydrogenation of furfural to furfuryl alcohol, *Catal. Today*. 279 (2017) 194–201, <https://doi.org/10.1016/j.cattod.2016.06.013>.
- [48] X. Chen, L. Zhang, B. Zhang, X. Guo, X. Mu, Highly selective hydrogenation of furfural to furfuryl alcohol over Pt nanoparticles supported on g-C<sub>3</sub>N<sub>4</sub> nanosheets catalysts in water, *Sci. Rep.* 6 (2016) 1–13, <https://doi.org/10.1038/srep28558>.
- [49] Y. Wang, P. Prinsen, K.S. Triantafyllidis, S.A. Karakoulia, P.N. Trikalitis, A. Yezec, C. Len, R. Luque, Comparative Study of Supported Monometallic Catalysts in the Liquid-Phase Hydrogenation of Furfural: Batch Versus Continuous Flow, *ACS Sustain. Chem. Eng.* 6 (8) (2018) 9831–9844, <https://doi.org/10.1021/acsschemeng.8b00984>.
- [50] A. Iriando, A. Mendiguren, M.B. Güemez, J. Reques, J.F. Cambra, 2,5-DMF production through hydrogenation of real and synthetic 5-HMF over transition metal catalysts supported on carriers with different nature, *Catal. Today*. 279 (2017) 286–295, <https://doi.org/10.1016/j.cattod.2016.02.019>.
- [51] W. Gong, C. Chen, Y. Zhang, H. Zhou, H. Wang, H. Zhang, Y. Zhang, G. Wang, H. Zhao, Efficient Synthesis of Furfuryl Alcohol from H<sub>2</sub>-Hydrogenation/Transfer Hydrogenation of Furfural Using Sulfonate Group Modified Cu Catalyst, *ACS Sustain. Chem. Eng.* 5 (3) (2017) 2172–2180, <https://doi.org/10.1021/acsschemeng.6b02343>.
- [52] Y. Shi, Y. Yang, Y.-W. Li, H. Jiao, Mechanisms of Mo<sub>2</sub>C(101)-Catalyzed Furfural Selective Hydrodeoxygenation to 2-Methylfuran from Computation, *ACS Catal.* 6 (10) (2016) 6790–6803, <https://doi.org/10.1021/acscatal.6b02000>.
- [53] F. Li, B.o. Cao, R. Ma, J. Liang, H. Song, H. Song, Performance of Cu/TiO<sub>2</sub>-SiO<sub>2</sub> catalysts in hydrogenation of furfural to furfuryl alcohol, *Can. J. Chem. Eng.* 94 (7) (2016) 1368–1374.
- [54] S. Sittitha, T. Sooknoi, Y. Ma, P.B. Balbuena, D.E. Resasco, Kinetics and mechanism of hydrogenation of furfural on Cu/SiO<sub>2</sub> catalysts, *J. Catal.* 277 (1) (2011) 1–13, <https://doi.org/10.1016/j.jcat.2010.10.005>.
- [55] R.M. Mironenko, O.B. Belskaya, T.I. Gulyaeva, A.I. Nizovskii, A.V. Kalinkin, V. I. Bukhtiyarov, A.V. Lavrenov, V.A. Likhobolov, Effect of the nature of carbon support on the formation of active sites in Pd/C and Ru/C catalysts for hydrogenation of furfural, *Catal. Today*. 249 (2015) 145–152, <https://doi.org/10.1016/j.cattod.2014.10.037>.
- [56] J.J. Musci, A.B. Merlo, M.L. Casella, Aqueous phase hydrogenation of furfural using carbon-supported Ru and RuSn catalysts, *Catal. Today*. 296 (2017) 43–50, <https://doi.org/10.1016/j.cattod.2017.04.063>.
- [57] L.J. Durndell, G. Zou, W. Shangquan, A.F. Lee, K. Wilson, Structure-Reactivity Relations in Ruthenium Catalysed Furfural Hydrogenation, *ChemCatChem* 11 (16) (2019) 3927–3932, <https://doi.org/10.1002/cctc.201900481>.
- [58] G. Bagnato, A. Figoli, C. Ursino, F. Galiano, A. Sanna, A novel Ru-polyethersulfone (PES) catalytic membrane for highly efficient and selective hydrogenation of furfural to furfuryl alcohol, *J. Mater. Chem. A*. 6 (12) (2018) 4955–4965.
- [59] P. Panagiotopoulou, D.G. Vlachos, Liquid phase catalytic transfer hydrogenation of furfural over a Ru/C catalyst, *Appl. Catal., A*. 480 (2014) 17–24, <https://doi.org/10.1016/j.apcata.2014.04.018>.
- [60] C.K.P. Neeli, Y.-M. Chung, W.-S. Ahn, Catalytic Transfer Hydrogenation of Furfural to Furfuryl Alcohol by using Ultrasmall Rh Nanoparticles Embedded on Diamine-Functionalized KIT-6, *ChemCatChem* 9 (24) (2017) 4570–4579, <https://doi.org/10.1002/cctc.201701037>.
- [61] E.-J. Ras, S. Maisuls, P. Haesackers, G.-J. Gruter, G. Rothenberg, Selective Hydrogenation of 5-Ethoxymethylfurfural over Alumina-Supported Heterogeneous Catalysts, *Adv. Synth. Catal.* 351 (18) (2009) 3175–3185, <https://doi.org/10.1002/adsc.200900526>.

- [62] V. Vetere, A.B. Merlo, J.F. Ruggera, M.L. Casella, Transition metal-based bimetallic catalysts for the chemoselective hydrogenation of furfuraldehyde, *J. Braz. Chem. Soc.* 21 (2010) 914–920, <https://doi.org/10.1590/S0103-50532010000500021>.
- [63] B.M. Matsagar, C.-Y. Hsu, S.S. Chen, T. Ahamad, S.M. Alshehri, D.C.W. Tsang, K.-W. Wu, Selective hydrogenation of furfural to tetrahydrofurfuryl alcohol over a Rh-loaded carbon catalyst in aqueous solution under mild conditions, *Sustain. Energy Fuels*. 4 (1) (2020) 293–301.
- [64] S. Liu, Y. Amada, M. Tamura, Y. Nakagawa, K. Tomishige, Performance and characterization of rhenium-modified Rh-Ir alloy catalyst for one-pot conversion of furfural into 1,5-pentanediol, *Catal. Sci. Technol.* 4 (8) (2014) 2535–2549.
- [65] M. Saliccioli, M. Stamatakis, S. Caratzoulas, D.G. Vlachos, A Review of Multiscale Modeling of Metal-Catalyzed Reactions: Mechanism Development for Complexity and Emergent Behavior, *Chem. Eng. Sci.* 66 (19) (2011) 4319–4355, <https://doi.org/10.1016/j.ces.2011.05.050>.
- [66] M.J. Gilkey, A.V. Mironenko, L. Yang, D.G. Vlachos, B. Xu, Insights into the Ring-Opening of Biomass-Derived Furanics over Carbon-Supported Ruthenium, *ChemSusChem* 9 (21) (2016) 3113–3121, <https://doi.org/10.1002/cssc.201600681>.
- [67] X. Cheng, D. Jiang, X. Hu, B. Barati, Y. Hu, L. Qian, S. Wang, H. Li, Mechanism of hydrothermal conversion of xylose to furfural in methanol solution: a study based on experiment and density functional theory, *J. Anal. Appl. Pyrolysis*. (2020), 104996, <https://doi.org/10.1016/j.jaap.2020.104996>.
- [68] M. Grilc, B. Likozar, Levulinic acid hydrodeoxygenation, decarboxylation and oligmerization over NiMo/Al<sub>2</sub>O<sub>3</sub> catalyst to bio-based value-added chemicals: Modelling of mass transfer, thermodynamics and micro-kinetics, *Chem. Eng. J.* 330 (2017) 383–397, <https://doi.org/10.1016/j.cej.2017.07.145>.
- [69] O. Mamun, E. Walker, M. Faheem, J.Q. Bond, A. Heyden, Theoretical Investigation of the Hydrodeoxygenation of Levulinic Acid to  $\gamma$ -Valerolactone over Ru(0001), *ACS Catal.* 7 (1) (2017) 215–228, <https://doi.org/10.1021/acscatal.6b0254810.1021/acscatal.6b02548.s001>.
- [70] O. Mamun, M. Saleheen, J.Q. Bond, A. Heyden, Importance of Angelica Lactone Formation in the Hydrodeoxygenation of Levulinic Acid to  $\gamma$ -Valerolactone over a Ru(0001) Model Surface, *J. Phys. Chem. C*. 121 (34) (2017) 18746–18761, <https://doi.org/10.1021/acs.jpcc.7b06369>.
- [71] S. Wang, V. Vorotnikov, D.G. Vlachos, Coverage-Induced Conformational Effects on Activity and Selectivity: Hydrogenation and Decarbonylation of Furfural on Pd (111), *ACS Catal.* 5 (1) (2015) 104–112, <https://doi.org/10.1021/cs5015145>.
- [72] Q.-X. Cai, J.-G. Wang, Y.-G. Wang, D. Mei, Mechanistic insights into the structure-dependent selectivity of catalytic furfural conversion on platinum catalysts, *AIChE J.* 61 (11) (2015) 3812–3824, <https://doi.org/10.1002/aic.14902>.
- [73] M.J. Gilkey, P. Panagiotopoulou, A.V. Mironenko, G.R. Jenness, D.G. Vlachos, B. Xu, Mechanistic Insights into Metal Lewis Acid-Mediated Catalytic Transfer Hydrogenation of Furfural to 2-Methylfuran, *ACS Catal.* 5 (7) (2015) 3988–3994, <https://doi.org/10.1021/acscatal.5b00586>.
- [74] A.V. Mironenko, D.G. Vlachos, Conjugation-Driven “Reverse Mars–van Krevelen”-Type Radical Mechanism for Low-Temperature C–O Bond Activation, *J. Am. Chem. Soc.* 138 (26) (2016) 8104–8113, <https://doi.org/10.1021/jacs.6b02871>.
- [75] R. Šivec, M. Grilc, M. Huš, B. Likozar, Multiscale Modeling of (Hemi)cellulose Hydrolysis and Cascade Hydrotreatment of 5-Hydroxymethylfurfural, Furfural, and Levulinic Acid, *Ind. Eng. Chem. Res.* 58 (35) (2019) 16018–16032, <https://doi.org/10.1021/acs.iecr.9b00898>.
- [76] A. Kojčinović, Ž. Kovacić, M. Huš, B. Likozar, M. Grilc, Furfural hydrogenation, hydrodeoxygenation and etherification over MoO<sub>2</sub> and MoO<sub>3</sub>: a combined experimental and theoretical study, *Appl. Surf. Sci.* 543 (2021) 148836, <https://doi.org/10.1016/j.apsusc.2020.148836>.
- [77] J. Lee, J.H. Seo, C. Nguyen-Huy, E. Yang, J.G. Lee, H. Lee, E.J. Jang, J.H. Kwak, J. H. Lee, H. Lee, K. An, Cu<sub>2</sub>O(100) surface as an active site for catalytic furfural hydrogenation, *Appl. Catal., B*. 282 (2021) 119576, <https://doi.org/10.1016/j.apcatb.2020.119576>.
- [78] A. Pavlišić, M. Huš, A. Prašnikar, B. Likozar, Multiscale modelling of CO<sub>2</sub> reduction to methanol over industrial Cu/ZnO/Al<sub>2</sub>O<sub>3</sub> heterogeneous catalyst: Linking ab initio surface reaction kinetics with reactor fluid dynamics, *J. Clean. Prod.* 275 (2020) 122958.
- [79] S. Flaischlen, G.D. Wehinger, Synthetic Packed-Bed Generation for CFD Simulations: Blender vs. STAR-CCM+, *ChemEngineering* 2019, Vol. 3, Page 52. 3 (2019) 52. <https://doi.org/10.3390/CHEMENGINEERING3020052>.
- [80] T. Eppinger, N. Jurtz, R. Aglave, Automated Workflow For Spatially Resolved Packed Bed Reactors With Spherical And Non-Spherical Particles, in: 10th Int. Conf. CFD Oil Gas, Metall. Process Ind., Trondheim, Norway, 2014.
- [81] A. Kokalj, T. Makino, M. Okada, DFT and TPD study of the role of steps in the adsorption of CO on copper: Cu(4 1 0) versus Cu(1 0 0), *J. Phys. Condens. Matter*. 29 (2017), 194001, <https://doi.org/10.1088/1361-648X/aa66a3>.
- [82] A. Bjelić, M. Grilc, M. Huš, B. Likozar, Hydrogenation and hydrodeoxygenation of aromatic lignin monomers over Cu/C, Ni/C, Pd/C, Pt/C, Rh/C and Ru/C catalysts: Mechanisms, reaction micro-kinetic modelling and quantitative structure-activity relationships, *Chem. Eng. J.* 359 (2019) 305–320, <https://doi.org/10.1016/j.cej.2018.11.107>.
- [83] J.V. Barth, Transport of adsorbates at metal surfaces: from thermal migration to hot precursors, *Surf. Sci. Rep.* 40 (2000) 75–149, [https://doi.org/10.1016/S0167-5729\(00\)00002-9](https://doi.org/10.1016/S0167-5729(00)00002-9).
- [84] R. Kosydar, I. Szewczyk, P. Natkański, D. Duraczyńska, J. Gurgul, P. Kuśrowski, A. Drelinkiewicz, New insight into the effect of surface oxidized groups of nanostructured carbon supported Pd catalysts on the furfural hydrogenation, *Surf. Interfaces* 17 (2019) 100379, <https://doi.org/10.1016/j.surfin.2019.100379>.
- [85] R. Ma, X.-P. Wu, T. Tong, Z.-J. Shao, Y. Wang, X. Liu, Q. Xia, X.-Q. Gong, The Critical Role of Water in the Ring Opening of Furfural Alcohol to 1,2-Pentanediol, *ACS Catal.* 7 (1) (2017) 333–337, <https://doi.org/10.1021/acscatal.6b02845>.